

Journal Pre-proofs

Synthesis, anticancer and antioxidant properties of new indole and pyranoindole derivatives

Domenico Iacopetta, Alessia Catalano, Jessica Ceramella, Alexia Barbarossa, Alessia Carocci, Alessia Fazio, Chiara La Torre, Anna Caruso, Marco Ponassi, Camillo Rosano, Carlo Franchini, Maria Stefania Sinicropi

PII: S0045-2068(20)31738-7
DOI: <https://doi.org/10.1016/j.bioorg.2020.104440>
Reference: YBIOO 104440

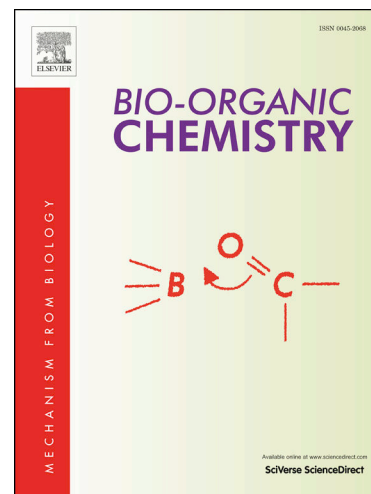
To appear in: *Bioorganic Chemistry*

Received Date: 20 August 2020
Revised Date: 30 September 2020
Accepted Date: 24 October 2020

Please cite this article as: D. Iacopetta, A. Catalano, J. Ceramella, A. Barbarossa, A. Carocci, A. Fazio, C. La Torre, A. Caruso, M. Ponassi, C. Rosano, C. Franchini, M. Stefania Sinicropi, Synthesis, anticancer and antioxidant properties of new indole and pyranoindole derivatives, *Bioorganic Chemistry* (2020), doi: <https://doi.org/10.1016/j.bioorg.2020.104440>

This is a PDF file of an article that has undergone enhancements after acceptance, such as the addition of a cover page and metadata, and formatting for readability, but it is not yet the definitive version of record. This version will undergo additional copyediting, typesetting and review before it is published in its final form, but we are providing this version to give early visibility of the article. Please note that, during the production process, errors may be discovered which could affect the content, and all legal disclaimers that apply to the journal pertain.

© 2020 Published by Elsevier Inc.



Synthesis, anticancer and antioxidant properties of new indole and pyranoindole derivatives

Domenico Iacopetta^{a,1}, Alessia Catalano^{b,1}, Jessica Ceramella^a, Alexia Barbarossa^b, Alessia Carocci^{b,*}, Alessia Fazio^a, Chiara La Torre^a, Anna Caruso^a, Marco Ponassi^c, Camillo Rosano^c, Carlo Franchini^b, Maria Stefania Sinicropi^a

^a*Department of Pharmacy, Health and Nutritional Sciences, University of Calabria, 87036, Arcavacata di Rende (Italy)*

^b*Department of Pharmacy-Drug Sciences, University of Bari "Aldo Moro", 70126, Bari (Italy)*

^c*Biopolymers and Proteomics IRCCS, Ospedale Policlinico San Martino-IST, Largo R. Benzi 10, 16132 Genova, Italy*

* *Corresponding author: e-mail address: alessia.carocci@uniba.it*

¹ *These authors equally contributed to this work.*

Abstract

The indole scaffold has been recognized, over the years, as a model for the synthesis of compounds with anticancer activity by dint of its substantiated ability to act via multiple mechanisms, which also involves the inhibition of enzymes engaged in DNA replication. In this regard, a new series of indole and pyranoindole derivatives have been prepared, some of which showed good antitumor activity and proved their inhibitory effects on the tubulin target. The anticancer activity of the newly synthesized compounds has been evaluated on breast cancer cell lines, as MCF-7 and MDA-MB231, cervical cancer cells line HeLa and Ishikawa endometrial cancer cell line. Among the compounds under study, **7** exhibited a good antitumor activity on HeLa cell line ($IC_{50} = 3.6 \pm 0.5$), leading to cell death by apoptosis due to the inhibition of tubulin polymerization, which demonstrated that the compound can explicate its function in a similar way to Vinblastine, a well-known inhibitor of tubulin polymerization. The data were also confirmed by *in silico* assays. No cytotoxicity against normal cells has been detected. Furthermore, in order to suggest a possible relationship between anticancer effects and to investigate the antioxidant properties, DPPH and ABTS tests were performed, together with fluorescence assays on 3T3-L1 cells. All our findings taken together led us to consider compound **7** a favourable candidate for the battle against cancer.

Key words: indole derivatives, tubulin, molecular docking studies, anticancers, antioxidants

Introduction

Despite the technological and social development, cancer is one of the most common diseases of concern and a leading cause of human suffering. It was estimated that deaths from cancer worldwide would rise over 13.1 million in 2030 (WHO report, Globocan 2012, IARC). Therefore, the design of newer and potent anticancer agents with higher selectivity on neoplastic cells and few side effects, able to overcome problems like severe toxicity as well as resistance with the existing drugs, may be envisaged. An ongoing source of debate is the possibility of some molecules with antioxidant properties to explicate chemopreventive action. Indeed, many prior studies corroborate that the antioxidants can enhance the known chemotherapy protocols by ameliorating the toxic side effects without affecting treatment efficacy [1]. Besides, other *in vitro* investigations suggest the relevant role of this kind of molecules in inducing the apoptosis in cancer cells [2]. In the last decades, research efforts resulted in the development of numerous antineoplastic agents with a variety of structures. Among them, the indole nucleus, due to its biodiversity and versatility, has been a highly privileged motif for the target-based design and development of anticancer agents [3]. Furthermore, FDA approved the use of some naturally occurring indole alkaloids for anti-tumor activity, including vinblastine (1961, breast cancer, choriocarcinoma, Hodgkin lymphoma, Kaposi sarcoma, mycosis fungoides, non-Hodgkin lymphoma, testicular cancer), vincristine (1963, leukemia), vinorelbine (1994, non-small cell lung cancer) and vindesine (1994, melanoma, lung cancers and uterine cancer) (Figure 1). Vinca alkaloids (vinblastine and vincristine) isolated from *Catharanthus roseus* (Apocynaceae) were the first plant alkaloids investigated for their use as anticancer agents [4]. They cause disruption of microtubules and arrest of cells in the metaphase, ultimately causing cell death by apoptosis. A number of semisynthetic analogues of vinblastine and vincristine, including vinorelbine and vindesine that are comparatively more effective, have been then developed [5].

Taking inspiration from these natural compounds, several synthetic analogues were synthesized, some of which showing good anti-tumor activity [6]. Recently, indole derivatives have been studied as inhibitors of enzymes involved in DNA replication as topoisomerase, telomerase, tubulin [7-9].

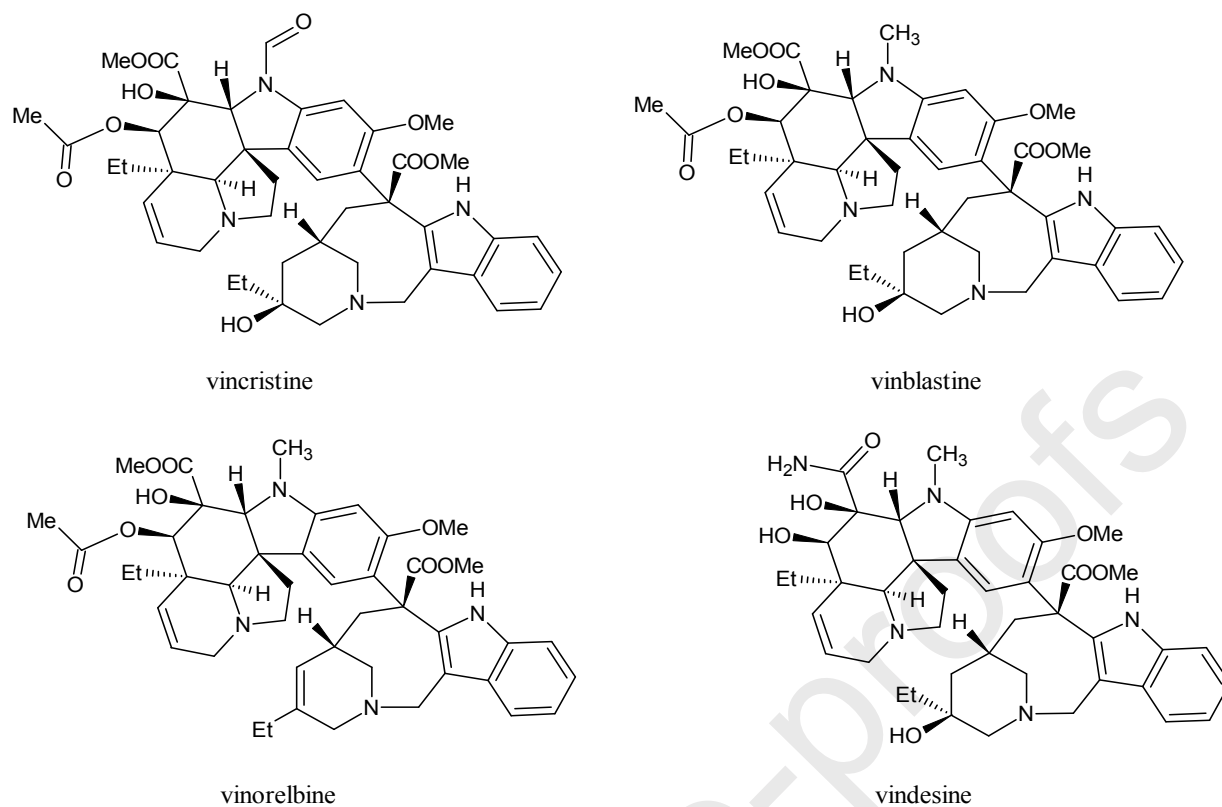


Figure 1. Structure of Vinca alkaloids

Due to the multiple functions of microtubules in cell mitosis, tubulin has become a highly attractive target for new anticancer drugs discovery [10]. Therefore, tubulin/microtubule-interacting drugs are used successfully for treatment of a wide variety of human cancers [11]. In the last decade, the synthesis and biological evaluation of some indole and corresponding pyranoindole derivatives (**I–IV**, Figure 2) was reported [12]. The compounds were evaluated for their inhibition of NO production, antioxidant activity and for their ability to inhibit *in vitro* the growth of four human tumor cell lines (large lung carcinoma COR-L23, alveolar basal epithelial carcinoma A549, amelanotic melanoma C32 and melanoma A375) [12]. Two indole derivatives (**I**, **II**) showed to be active against amelanotic melanoma cell lines, while inhibiting NO production in murine monocytic macrophage. Moreover, several researches highlighted the ability of indole derivatives to suppress the proliferation of a large panel of tumor cells, including breast and uterine cancer cells. In particular, it was reported that indole-3-carbinol and its metabolite exerted a potent effect in cervical cancer and in human Ishikawa endometrial cancer cells [13, 14]. In addition, the same compounds caused a selective cell

growth inhibition and induction of apoptosis in several breast tumor cells (MDA-MB-468, MCF-7 and MDA-MB-231) [15] [16]. More recently, Prasad et al also demonstrated the capability of three 2-amino-2-(1H-indole-2-yl) derivatives to suppress the proliferation of breast cancer cell lines, MCF-7 and MDA-MB-231 [17].

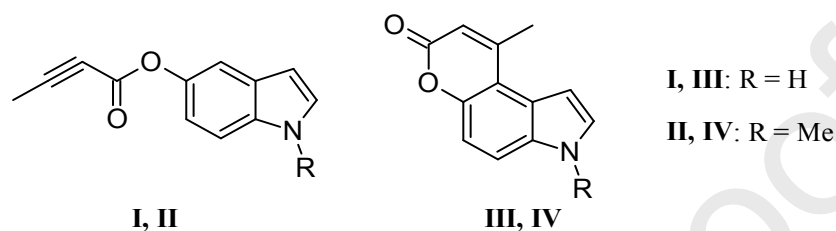


Figure 2. Structure of indoles (**I, II**) and pyranoindoles (**III, IV**) described in the literature

Based on these evidences, new indole and pyranoindole derivatives (**5–13**, Figure 3) have been synthesized in order to enlarge studies on this class of compounds towards the breast and uterine cancer cells, representing the leading cause of death in women [18]. Thus, the anticancer activity on breast cancer (MCF-7 and MDA-MB-231) and human uterine carcinoma cell lines (HeLa and Ishikawa) of these new compounds is reported herein, along with the evaluation of their ability to inhibit tubulin microtubule polymerization. Furthermore, ~~in order to delve into the possible relationship between the antioxidant properties and anticancer mechanisms,~~ the antioxidant activity of the synthesized compounds have been evaluated by means of both *in vitro* and cellular assay. Finally, molecular docking studies have also been conducted to support the results obtained.

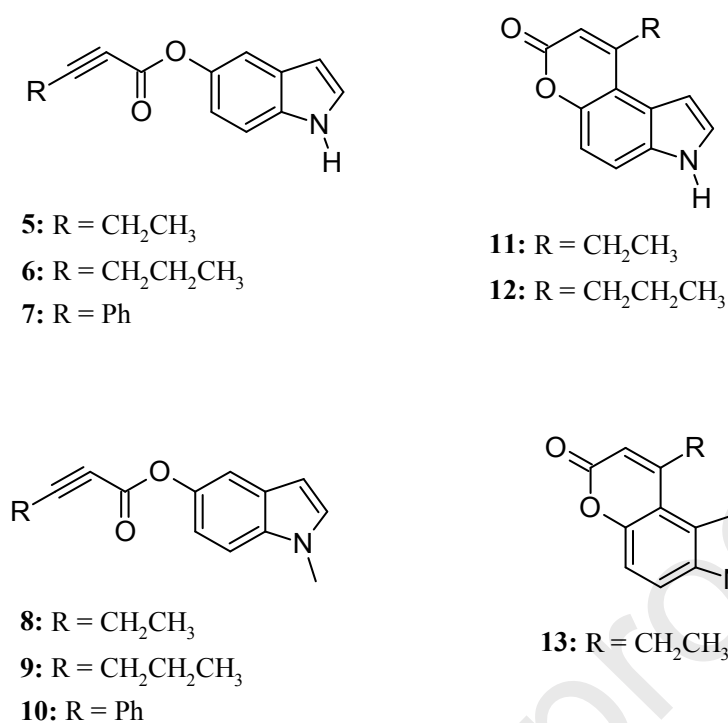
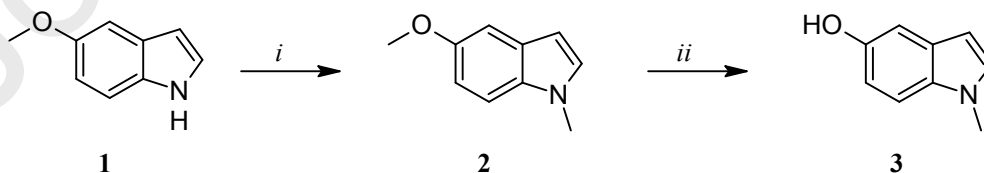


Figure 3. Structure of indoles (**5–10**) and pyranoindoles (**11–13**) under study.

2. Results and Discussion

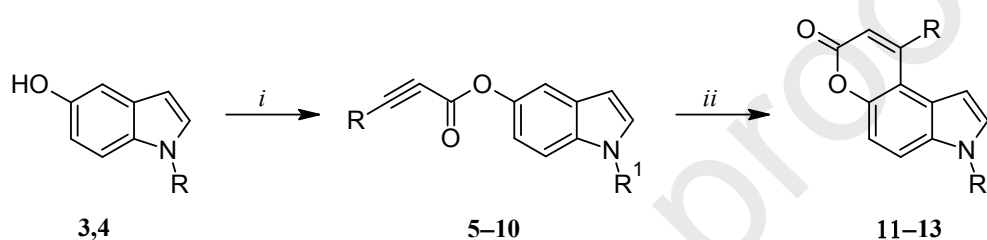
2.1. Chemistry

The synthesis of 5-hydroxy-1-methylindole **3** is depicted in Scheme 1. 5-Methoxyindole **1** was treated with NaH to obtain the *N*-anion followed by reaction with methyl iodide to give 5-methoxy-1-methylindole **2**. Selective demethylation of the methoxy group by heating compound **2** with anhydrous pyridine hydrochloride gave the desired **3** [12].



Scheme 1. Reagents and conditions: (i) NaH 60% oil dispersion, CH₃I, DMF, 0 °C→rt, 1 h (81%); (ii) pyridine hydrochloride, Δ, 3 h (46%).

The synthesis of the indole and pyranindole derivatives is depicted in Scheme 2. Commercial 5-hydroxyindole **4** was submitted to esterification with pent-2-ynoic acid, es-2-ynoic acid or phenylpropionic acid to give the corresponding esters **5**, **6**, **7**, respectively. The same reactions, run on 5-hydroxy-1-methylindole **3** gave esters **8**, **9**, **10**. When esters **5**, **6**, **8** were heated under reflux in dioxane-dichloroethane in the presence of PtCl_4 as a catalyst, an intramolecular cyclization occurred giving pyranindoles **11**, **12**, **13**, respectively, as confirmed by NMR analyses.



Scheme 2. Reagents and conditions: (i) pent-2-ynoic acid (for compounds **5** and **8**, 48% and 40%, respectively) or es-2-ynoic acid (for compounds **6** and **9**, 42% and 11%, respectively) or phenylpropionic acid (for compounds **7** and **10**, 40% and 34%, respectively), DCC, DMAP, $\text{CH}_2\text{Cl}_2/\text{DMF}$ (10:1), rt, 4 h; (ii) PtCl_4 , 1,4-dioxane/1,2-dichloroethane (1:1), reflux, 5 h (55%, 16% and 62%, for **10**, **11** and **13**, respectively).

2.1.1 Thermal stability test

Prior research has thoroughly investigated the possibility of several organic compounds to decompose by heat action[19]. Compound **7**, the most bioactive molecule of the series, presents in its structure a triple bond, a possible source of molecular instability. For this reason, through the modification of already known protocols aimed at verifying heat stability, we performed a “stress test assay” on **7** by heating it for 6 hours at 60 °C. At the end of the process, we compared the NMR spectra of **7** in the usual conditions and after the heat treatment. The match of the two spectra surmises that **7** is heat resistant.

2.2. Biological Results

2.2.1 Cell viability assay

The cytotoxic activities of synthesized compounds were evaluated against four human cancer cell lines, including two breast cancer cells (MCF-7 and MDA-MB-231) and two human uterine cancer cells (HeLa and Ishikawa), using MTT assay. The calculated IC_{50} values of studied compounds in comparison with the reference drug, Vinblastine, are listed in Table 1. Among them, the indole bearing the phenylpropionic group, compound **7**, exhibited the best anticancer activity, particularly toward the human cervical cancer cells HeLa and the breast cancer cells MCF-7, with the IC_{50} values amounting to 3.6 ± 0.5 and 3.8 ± 0.7 μM , respectively (dose response curve is shown in Figure 11 of supplementary materials). A moderate anticancer activity toward all the cell lines used was also shown by compounds **5** and **6**, mostly toward HeLa cells ($IC_{50} = 9.8 \pm 0.3$ and 14.5 ± 0.6 μM , respectively). Compounds **5** and **6** are structurally indole analogues of compound **7**, bearing the pent-2-ynoyl and *es*-2-ynoyl groups, respectively. The methylindole derivatives **8**, **9** and **10** possessed a lower activity than the indole analogues, except for methylindole **8** that showed an interesting anticancer activity, in particular against the uterine cancer cells Ishikawa and HeLa ($IC_{50} = 13.1 \pm 0.3$ and 14.0 ± 0.7 μM , respectively). Thus, the addition of a methyl group on the nitrogen indole ring appears to cause a decrease in antiproliferative activity. Moreover, the pyranoindole compounds **11**, **12** and **13** exhibited a lower or no antiproliferative activity on the cell lines tested, highlighting the importance of the indole group in the moiety of these compounds. The known microtubule-binding agent Vinblastine showed a stronger anticancer activity than our synthesized compounds on all cancer cell lines, with IC_{50} values between $2.3 \times 10^{-2} \pm 0.6$ μM and $1.6 \times 10^{-1} \pm 0.3$ μM . However, Vinblastine exhibited also a dramatic cytotoxic effect on normal cells used in this assay (MCF-10A, Hek-293 and 3T3-L1), unlike our compounds that did not interfere with the normal cells viability, at least until the concentration of 200 μM and under the conditions used for this assay.

Table 1. IC₅₀ values of compounds **5-13** and Vinblastine expressed in μM^{a} .

Compounds	MCF-7	MDA-MB-231	HeLa	Ishikawa	MCF-10A	Hek-293	3T3-L1
5	13.1±0.3	10.7±0.2	9.8±0.3	12.1±0.6	>200	>200	>200
6	30.2±0.2	15.9±0.5	14.5±0.6	30.5±0.5	>200	>200	>200
7	3.8±0.7	9.9±0.3	3.6±0.5	10.1±0.7	>200	>200	>200
8	23.0±0.4	23.5±0.4	14.0±0.7	13.1±0.3	>200	>200	>200
9	>200	>200	>200	>200	>200	>200	>200
10	37.6±0.5	40.7±0.8	49.5±0.9	77.7±0.4	>200	>200	>200
11	86.0±0.3	44.4±0.3	21.1±0.7	84.0±0.5	>200	>200	>200
12	>200	172.4±0.6	141.4±0.7	>200	>200	>200	>200
13	131.5±0.3	80.2±0.5	>200	>200	>200	>200	>200
Vinblastine	4.5x10 ⁻² ±0.6	1.6x10 ⁻¹ ±0.3	6.7x10 ⁻² ±0.5	2.5x10 ⁻² ±0,7	2.3x10 ⁻² ±0.6	80.8±0.4	1.9x10 ⁻⁴ ±0.8

^aValues are the mean of at least three determinations performed in triplicate.

2.2.2 Effect of compound 7 on microtubule dynamics and cell death by apoptosis

Numerous studies have shown that the alteration of microtubule dynamics induced by different compounds causes mitochondrial membrane potential activation, cell cycle and mitotic process arrest [11, 20-22]. To demonstrate the specific action of the synthesized compounds on tubulin network, we chose compound **7** and performed an immunofluorescence test using the anti- β -tubulin antibody on HeLa cells, on which compound **7** displayed the best antiproliferative activity. In Figure 4, the vehicle-treated cells (panel A, CTRL) showed a normal distribution of the microtubule network, with intact tubulin polymers regularly distributed throughout the cytoplasmic region (panel B, CTRL). After only 24 hours of compound **7** treatment (used at its IC₅₀ value), tubulin microfilaments appeared as distinct punctiform structures and accumulates unfairly throughout the cell cytoplasm and nucleus (Panel B, compound **7**, see white arrows). A similar behavior can be observed in Figure 3, Panel B, Vinblastine, where microtubules became irregular and the arrangement and organization of the tubulin network showed a severe disruption with a stronger formation of dot-like structures.

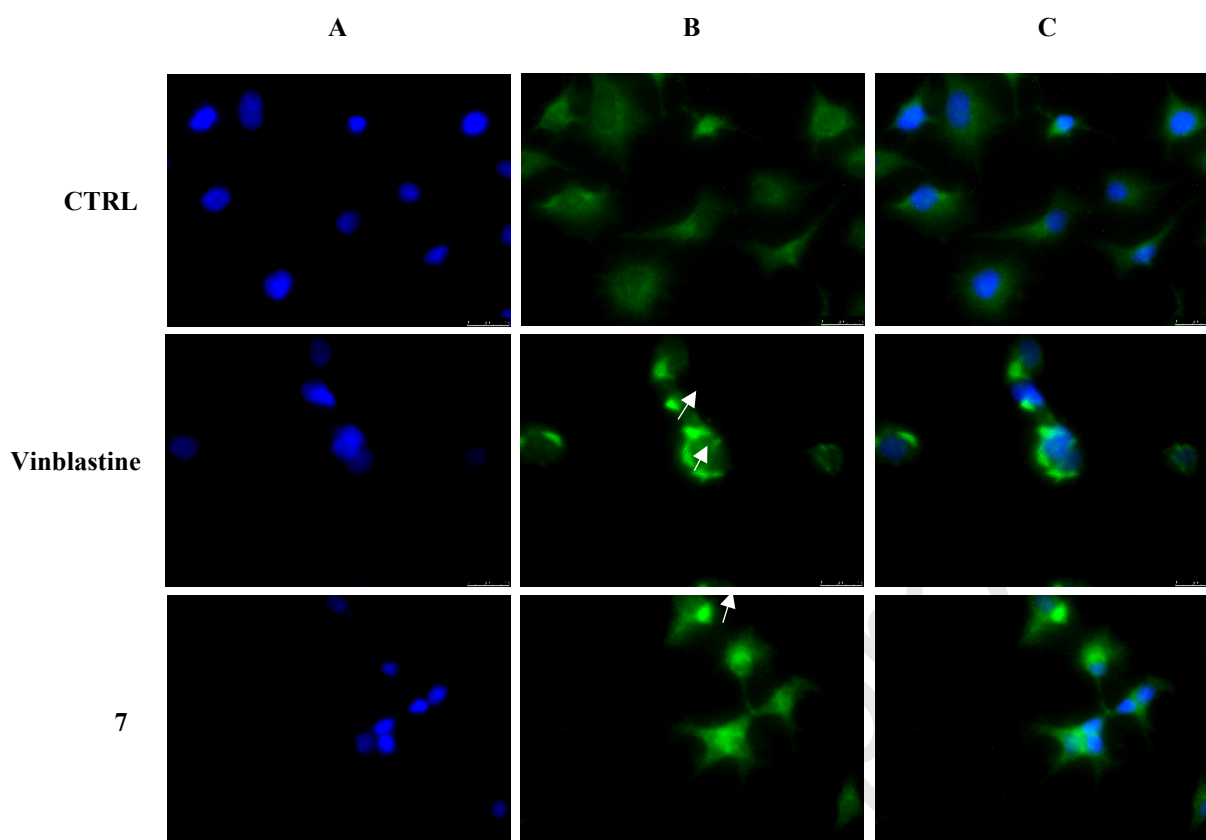


Figure 4. Immunofluorescence studies. HeLa cells were treated with the compound **7** or with Vinblastine (both used at their IC_{50} values) or with a vehicle (CTRL) for 24 h. After treatment, the cells were incubated with antibodies and observed under the inverted fluorescence microscope at $63\times$ magnification, as in depth described in Materials and Methods. Vehicle-treated HeLa cells (CTRL) exhibited a normal arrangement and organization of the cytoskeleton. Instead, HeLa cells treated with compound **7** and Vinblastine showed an irregular arrangement and organization of tubulin. Panels A: DAPI ($\lambda_{ex} = 350 \text{ nm}/\lambda_{em} = 460 \text{ nm}$); Panels B: β -tubulin (Alexa Fluor® 488; $\lambda_{ex} = 490 \text{ nm}/\lambda_{em} = 515 \text{ nm}$); Panels C: show the overlay channels. Representative fields are shown. DAPI ($\lambda_{ex} = 350 \text{ nm}/\lambda_{em} = 460 \text{ nm}$); Panels B: β -tubulin (Alexa Fluor® 488; $\lambda_{ex} = 490 \text{ nm}/\lambda_{em} = 515 \text{ nm}$); Panels C: show the overlay channels. Representative fields are shown.

To confirm these data, we examined the effect of compound **7** on the tubulin polymerization using a specific *in vitro* assay and measuring the turbidity variation every 30 seconds at 350 nm for 90 minutes. We used two well-known compounds as reference molecules, a tubulin polymerization inhibitor, Vinblastine, and a stabilizing agent, Paclitaxel. In the only vehicle (CTRL) reaction, tubulin heterodimers rapidly self-assembled to form linear tubulin polymers, in a time-dependent manner, with a final optical density (OD_{350}) of above 0.44, as showed in Figure 5. The microtubule-stabilizing agent Paclitaxel caused an increased rate of tubulin heterodimers assembly, whereas using the

microtubule-destabilizing agent such Vinblastine, the polymerization reaction was hampered (final OD₃₅₀ of 0.19). Compound **7** interfered with the tubulin polymerization with a similar effectiveness to Vinblastine, indeed the polymerization curve reached the steady state at an OD₃₅₀ 1.5-fold lesser than the control reaction (OD₃₅₀ = 0.48 and 0.3 for CTRL and compound **7**, respectively), with a final OD₃₅₀ value of about 0.24. Thus, compound **7** resulted an inhibitor of tubulin polymerization.

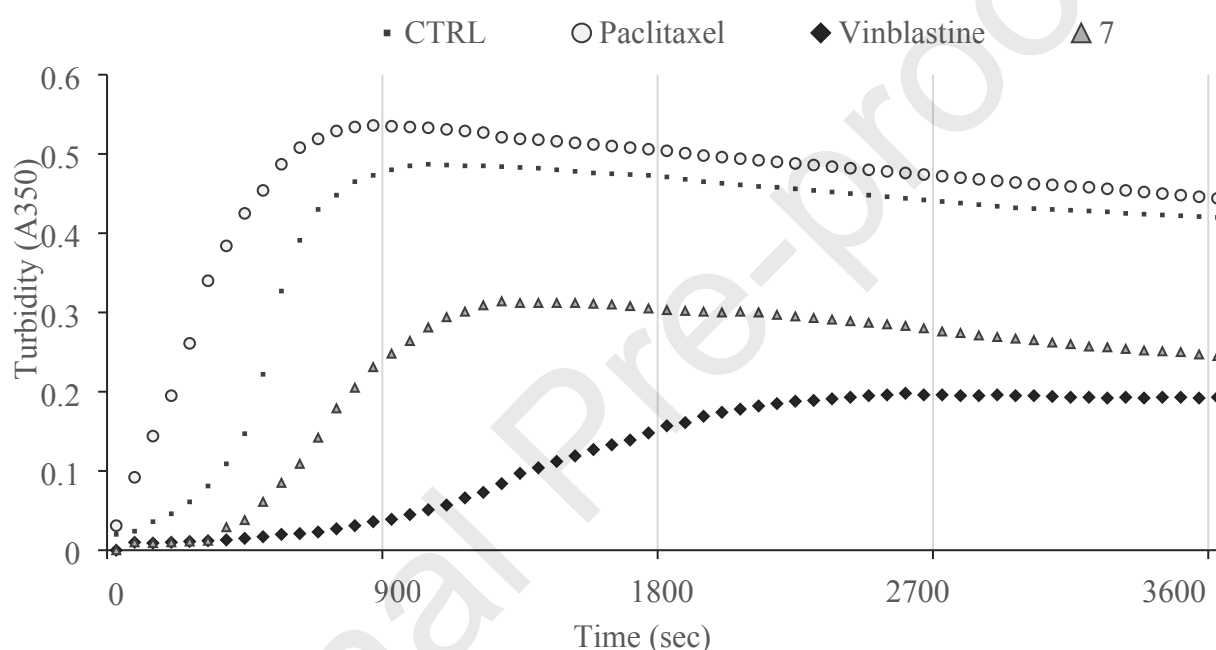


Figure 5. Tubulin-polymerization assay. The effect of compound **7** on *in vitro* tubulin polymerization was evaluated by measuring the turbidity variation at 350 nm for 3600 s, as described in the experimental section. Paclitaxel and Vinblastine were used, at a concentration of 10 μ M, as tubulin-stabilizing and tubulin-destabilizing agents, respectively. DMSO was used as a negative control.

The alteration of microtubules network causes a blockage of the mitotic process progression with the induction, in the last phase, of the apoptotic process [23, 24]. For this reason, we decided to perform a TUNEL assay with the aim to demonstrate the ability of compound **7** to induce cell death by apoptosis on the HeLa tumor cell line. The induction of apoptosis promotes morphological characteristic changes such as the cellular narrowing (the cytoplasm is dense and the organelles are narrower), the picnosis, which is the result of the condensation of the chromatin, and the fragmentation of the DNA[25]. The experiment was conducted by treating HeLa with compound **7**,

used at its IC_{50} value, or with the vehicle (DMSO) for 24 h, and then performing the TUNEL assay, as described in the materials and methods section. The images obtained (Figure 6) clearly show the development of a nuclear green fluorescence in the cells treated with compound **7**, due to DNA damage related to the apoptotic process. This fluorescence, however, is absent in the cells treated with the vehicle only (Panel B, CTRL) used as control.

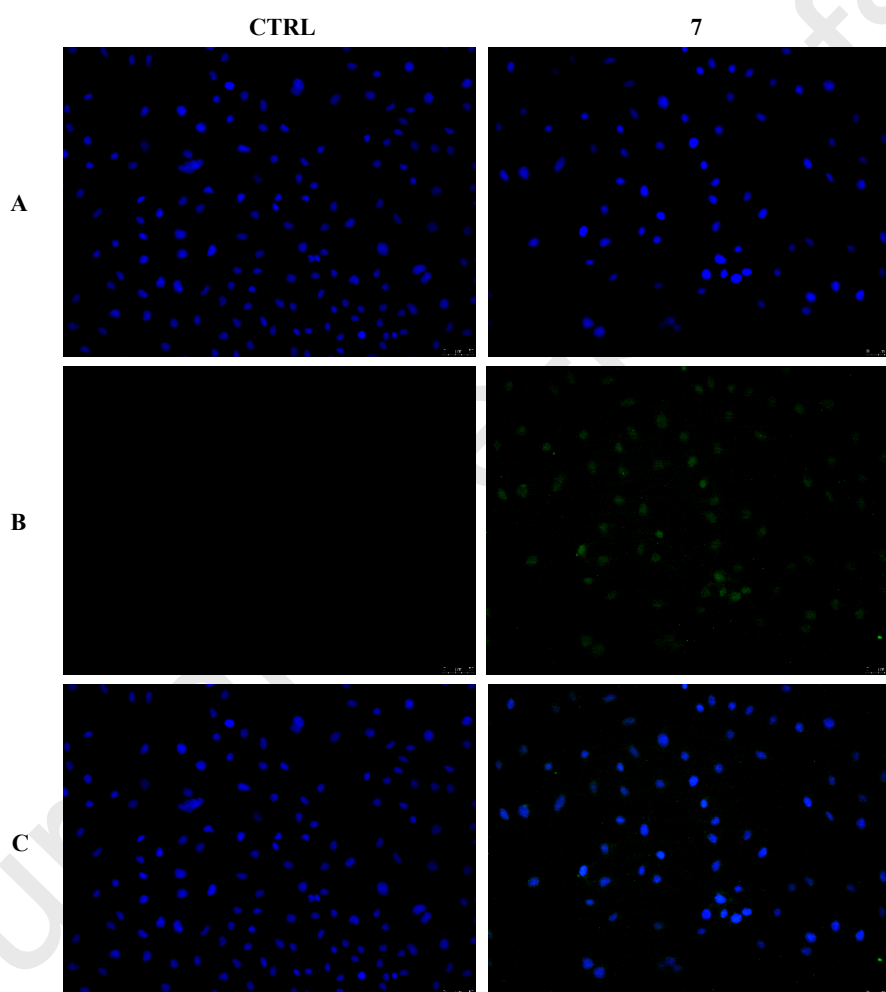


Figure 6. TUNEL assay. HeLa cells were treated with compound **7** at its IC_{50} value or with vehicle (CTRL) for 24 h. After treatment, cells were incubated with rTdT enzyme reaction and then observed and imaged under an inverted fluorescence microscope at 20x magnification (see materials and methods). The green nuclear fluorescence, visible in cells treated with compound **7**, and absent in the CTRL cells, indicates the apoptotic death. Panels A: DAPI ($\lambda_{ex} = 350$ nm/ $\lambda_{em} = 460$ nm); Panels B: CFTM488A ($\lambda_{ex} = 490$ nm/ $\lambda_{em} = 515$ nm) Panels C: show the overlay. Fields are representative of three separate experiments.

It is known that reactive oxygen species (ROS), at low doses, are essential for regulation of normal physiological functions of the cells. However, high cellular levels of ROS cause serious damages to proteins, nucleic acids, lipids, membranes and others organelles, which can lead to trigger cell death pathway such as apoptosis [26]. Considering the main role of ROS in the regulation of the apoptosis process, we investigated whether the most active compound **7** could act as ROS scavenger in a non-tumoral cell model, the mouse fibroblasts 3T3-L1, by using fluorescence assays. In particular, we treated 3T3-L1 with compound **7** at a concentration of 10 μ M for 24 h and then we induced ROS production treating with menadione (Men) for 1 h at 40 μ M. At the end of the treatment cells were incubated with 2',7'-dichlorofluorescein diacetate (DCFH-DA) for 2 h. DCFH-DA is hydrolyzed by cellular esterases to 2',7'-dichlorodihydrofluorescein and, then, oxidized to the green fluorescent 2',7'-dichlorofluorescein (DCF) by intracellular H_2O_2 . The green fluorescence was then observed and imaged under a fluorescence microscope. The obtained results, showed in Figure 7, highlighted that the pre-treatment with compound **7** significantly reduced the oxidative stress induced by menadione (Figure 7a, panel B, **7**+Men), if compared with the cells treated only with menadione (Figure 6a, panel B, Men). The quantification of the green fluorescence (Figure 7b) demonstrated, in fact, that compound **7** was able to cause a three-fold decrease of ROS generation in the 3T3-L1 cells, acting as a good scavenging of ROS.

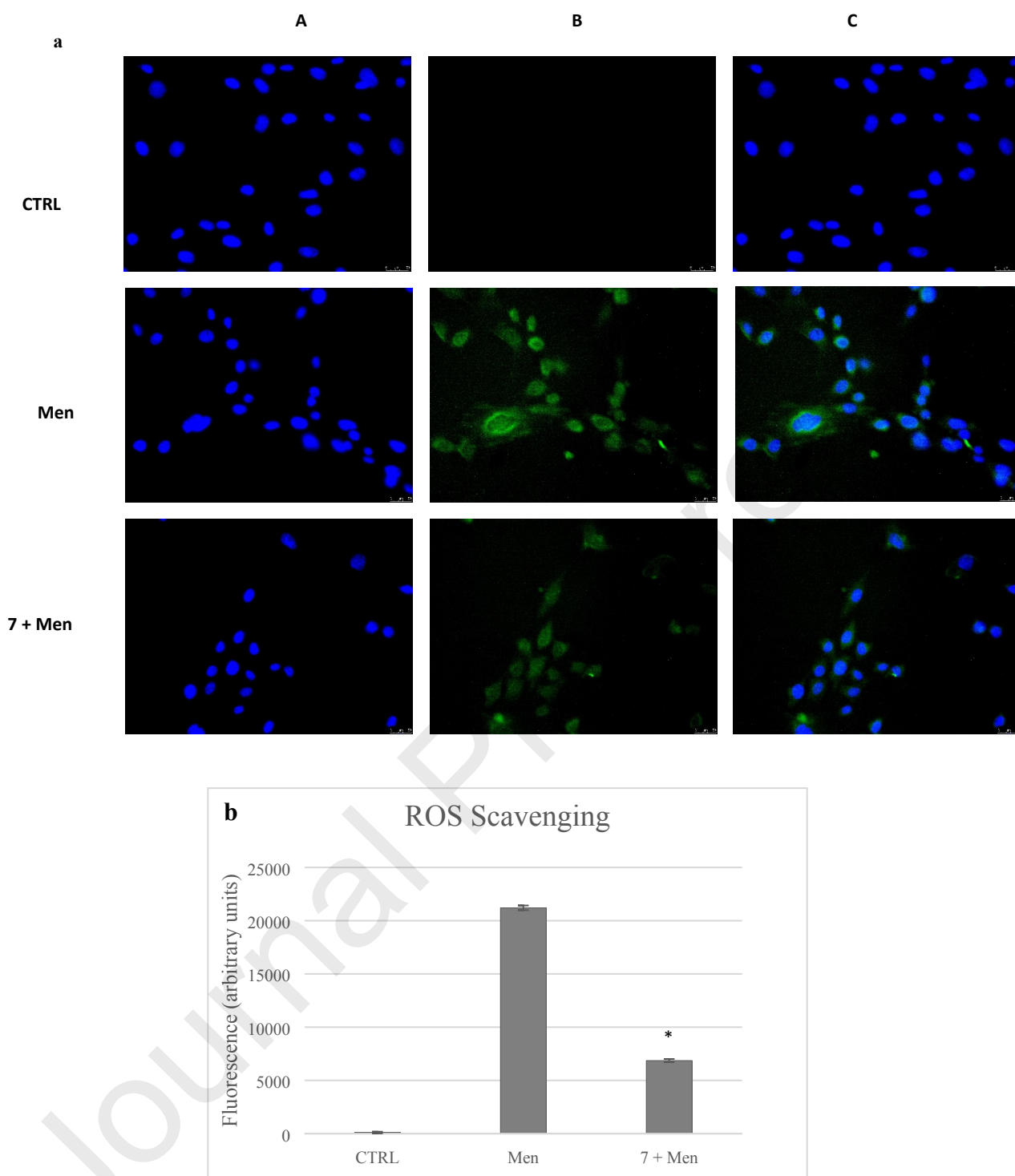


Figure 7. ROS scavenging activity. **(a)** Evaluation of ROS scavenging activity using DCF-DA (CFTM488A), in 3T3-L1 cells treated with compound **7** and Men (used as ROS inducer). Images were acquired at 20x magnification. The pre-treatment with compound **7** causes a 3-fold reduction of ROS production induced by Men (Figure 6a, panels **B**, **7 + Men**). Panels **A**: 2-(4-amidinophenyl)-6-indolecarbamide dihydrochloride (CTRL, Men, **7 + Men**) $\lambda_{ex/em}$ = 350 nm/460 nm. Panels **B**: CFTM488A (CTRL, Men, **7 + Men**,) $\lambda_{ex/em}$ = 490 nm/515 nm. Panels **C** (CTRL, Men, **7 + Men**) show the overlay channel. **(b)** Fluorescence quantification; * $p < 0.001$, **7 + Men** versus Men.

2.3 *In vitro* antioxidant activity

The radical scavenging activity of the synthesized compounds against the two most commonly used stable radicals (DPPH• and ABTS•⁺) was evaluated by *in vitro* studies.

2.3.1 DPPH assay

The free radical scavenging activity against DPPH was determined for all compounds under study (**5-13**). The DPPH assay, which is based on the reduction of the purple DPPH to 1, 1-diphenyl-2-picryl hydrazine (DPPH-H) via hydrogen transfer (HT) mechanisms, measures the ability of antioxidant compounds for trapping free radicals by donating hydrogen atoms, producing in consequence the bleaching of the colored radical solutions.

The results obtained as a function of concentration (8.33, 3.33, 1.67, 0.33 $\mu\text{g mL}^{-1}$) were reported in Table 2 (Figure 8 in supporting information). The results showed that the scavenging effects of the compounds on DPPH radical increased with the concentration. The data indicated that, among the synthetic compounds, **6** with the inhibition percentage of 90.45% at the highest concentration (8.33 $\mu\text{g mL}^{-1}$), displayed higher antioxidant activity than the other compounds. Compound **6** exhibited a high value of antioxidant ability even at lower concentration (78.2% at 1.67 $\mu\text{g mL}^{-1}$). Compounds **9** and **10** showed moderate antioxidant activities (79.04 and 73.40 %, respectively, at the highest concentration).

Compounds **7** and **12** showed a DPPH inhibition percentage of 43% and 50% at the highest concentration. The lowest antioxidant activity with a DPPH inhibition value of 10% at 8.33 $\mu\text{g mL}^{-1}$ belongs to **8**. Compound **11** was the only compound that did not exhibit any antioxidant activity at the lowest concentration tested (0.33 $\mu\text{g mL}^{-1}$).

The antioxidant activity does not appear to rely on the presence or absence of a methyl group onto the indole nitrogen atom, but it seems to depend mostly on the alkyl or aryl group in the side chain of the tested compounds. From our results it seems that the presence of a *n*-propyl group is crucial for antioxidant activity both in the series of indoles and pyranoindoles (see compounds **6**, **9** and **12**),

followed by the phenyl one (compounds **7** and **10**). On the contrary, the methyl group is detrimental for this activity (see compounds **5**, **8**, **11** and **13**).

Table 2. %I_{DPPH} of compounds **5–13** ± standard deviation

Compound	Concentration (µg mL ⁻¹)			
	8.33	3.33	1.67	0.33
Trolox	99.0±0	93.33±0.51	92.68±0.53	92.68±0.53
5	36.02±0.78	32.02±2.85	30.13±0.69	17.75±0.53
6	90.45±0.52	87.96±1.06	78.18±0.54	24.90±2.98
7	43.25±1.36	31.42±3.48	26.58±3.52	5.96±1.35
8	10.44±1.61	6.93±1.22	4.81±0.76	2.02±0.76
9	79.04±2.69	49.11±1.68	35.00±2.14	11.83±3.65
10	73.40±0.30	42.96±3.08	24.76±4.69	11.80±0.45
11	35.60±2.21	26.83±1.47	11.23±0.41	0
12	50.53±0.25	37.72±3.27	28.16±1.38	21.48±0.40
13	14.39±1.66	15.25±0.90	13.16±0.25	9.55±2.79

Antioxidant capacities were also expressed as Trolox equivalent antioxidant capacity (TEAC). The results reported in Table 3 highlighted that **6** was the compound with the highest antioxidant activity at all concentrations (from 37.90±8.25 at 0.33 µg mL⁻¹ to 219.56±1.43 at 8.33 µg mL⁻¹), while lowest TEAC value results from **8** (2.90±0.02 at 8.33 µg mL⁻¹).

Table 3. DPPH radical scavenging of compounds **5–13** expressed as μg of TE/g DW

Compound	Concentration ($\mu\text{g mL}^{-1}$)			
	8.33	3.33	1.67	0.33
5	70.05 \pm 2.17	59.08 \pm 7.87	53.86 \pm 1.89	19.81 \pm 1.49
6	219.56 \pm 1.43	212.67 \pm 2.96	185.52 \pm 1.48	37.90 \pm 8.25
7	89.56 \pm 3.78	43.60 \pm 9.74	56.94 \pm 9.58	0
8	2.90 \pm 0.02	0	0	0
9	189.09 \pm 7.28	107.91 \pm 4.58	69.56 \pm 5.85	6.70 \pm 0.89
10	173.62 \pm 0.81	90.75 \pm 8.36	41.22 \pm 12.77	6.00 \pm 1.24
11	71.23 \pm 5.98	47.43 \pm 3.96	5.05 \pm 1.08	0
12	111.71 \pm 0.70	76.94 \pm 8.86	51.00 \pm 0.14	32.90 \pm 1.08
13	13.62 \pm 4.54	16.00 \pm 2.46	10.29 \pm 0.72	0.51 \pm 0.02

In order to furtherly assess which extracts have the greatest antioxidant activity, EC_{50} values were determined (Table 4). Low EC_{50} values reflect a strong ability of the molecule to act as a DPPH scavenger whereas a high EC_{50} value indicates low scavenging activity of the scavengers, as more amount of the scavengers was required to achieve 50 % scavenging reaction. Consequently, the scavengers are less effective at scavenging DPPH radicals. Data obtained showed that the order of reactivity found was **6** > **9** > **10** > **12** > **7** > **5** > **11** > **13** > **8**. Considering these findings, it is possible to confirm that the compound **6** is the compound with the highest DPPH radical scavenging capacity while the compound **8** is a poor DPPH radical scavenger.

Table 4. EC₅₀ values of compounds **5–13** expressed in $\mu\text{g mL}^{-1} \pm$ standard deviation

Compound	EC ₅₀ ± SD
Trolox	0.04±0.01
5	8.67 ± 1.21
6	0.66 ± 0.2
7	8.30 ± 2.43
8	61.76 ± 2.36
9	2.96 ± 0.54
10	4.00 ± 0.12
11	12.79 ± 1.17
12	5.76 ± 1.32
13	32.55 ± 1.41

2.3.2 ABTS assay

The free radical scavenging activity against ABTS (2,2'-azino-bis(3-ethylbenzothiazoline-6-sulfonate)) was determined at four different concentrations (2.5, 1.0, 0.5 and 0.1 mg mL⁻¹ in DMSO) and it is shown in Table 5 (Figure 9 in supporting information). All the derivatives exhibited a lower capacity to inhibit the cationic radical ABTS^{•+} than the DPPH radical. Similarly to-DPPH assay, the scavenging effects of the compounds on cationic radical ABTS^{•+} increased with the compound concentration. An opposite trend was observed for the ABTS assay, where **9** and **10** had higher scavenging activity (30.34% and 21.56, respectively) than **6** (14.96%). The antioxidant ability determined by *in vitro* assays can significantly differ[27] but the combination of the results obtained from these two assays is considered of higher significance for a reliable evaluation of compounds radical scavenging capacity than the use of only one method. The ABTS assay is based on the *in situ* generation of a blue/green radical (ABTS^{•+}) that can be reduced by antioxidants by either single

electron transfer (SET) or hydrogen transfer (HT) mechanisms, whereas the DPPH assay is based on its reduction to 1,1-diphenyl-2-picryl hydrazine (DPPH-H) via HT mechanism.

6 at the highest concentration did not exceed 15 % of inhibitory activity, while recording the zero at the lowest concentration. For all the other tested molecules no important inhibitory activity was highlighted and **11, 8, 13** were confirmed as the least active compounds also against the radical cation ABTS^{•+}.

Table 5. %I_{ABTS} of compounds **5–13** ± standard deviation

Compound	Concentration (µg mL ⁻¹)			
	25	10	5	1
Trolox	99.00±0	99.04±0.41	51.52±1.33	18.81±0.65
5	4.82±0.48	3.12±0.51	2.36±0.28	1.18±0.69
6	14.96±0.33	3.43±0.33	2.36±0.07	0
7	11.59±0.16	5.89±0.70	4.62±0.33	0.58±0.02
8	3.52±1.56	3.13±1.17	2±0.73	0
9	30.34±1.35	15.98±1.96	6.86±0.57	2.85±2.01
10	21.56±1.48	8.86±1.38	3.81±0.28	1.67±0.51
11	1.26±0.24	0	0	0
12	5.25±0.27	4.12±0.66	3.22±0.14	0.59±0.38
13	2.51±0.5	0.51±0.03	0	0

Antioxidant capacities were also expressed as Trolox equivalent antioxidant capacity (TEAC) (Table 6). The results highlighted that the values were very low even for the **9** which showed the highest ABTS inhibition percentage among all the compounds (2.07% at 8.33 µg mL⁻¹).

Table 6. ABTS radical scavenging of compounds **5–13** expressed as μg of TE/g DW

Compounds	Concentration ($\mu\text{g mL}^{-1}$)			
	25	10	5	1
5	0.34 \pm 0.04	0.21 \pm 0.04	0.16 \pm 0.02	0.07 \pm 0.04
6	1.10 \pm 0.02	0.23 \pm 0.02	0.15 \pm 0.01	0
7	0.63 \pm 0.01	0.17 \pm 0.06	0.07 \pm 0.03	0.58 \pm 0.02
8	0.31 \pm 0.12	0.28 \pm 0.09	0.18 \pm 0.06	0
9	2.07 \pm 0.11	0.94 \pm 0.16	0.22 \pm 0.03	0
10	1.67 \pm 0.11	0.71 \pm 0.11	0.33 \pm 0.01	0.17 \pm 0.10
11	0.07 \pm 0.02	0	0	0
12	0.07 \pm 0.02	4.12 \pm 0.66	3.22 \pm 0.14	0.59 \pm 0.38
13	0.22 \pm 0.18	0.07 \pm 0.08	0.03 \pm 0	0.03 \pm 0

The EC_{50} values for the ABTS inhibition percentage are shown in Table 7. Data highlighted that the order of compound reactivity was **9** > **10** > **6** > **12** > **7** > **9** > **8** > **13** > **11**, thus **9** and **11** are the compounds with the highest and lowest ABTS radical scavenging, respectively.

Table 7. EC₅₀ values expressed in $\mu\text{g mL}^{-1} \pm$ standard deviations

Molecules	EC ₅₀ ± DS
<i>Trolox</i>	2.20±0.12
5	435.5 ± 0.5
6	156.6 ± 0.7
7	178.5 ± 1.0
8	560.5 ± 0.9
9	54.96 ± 1.48
10	92.33 ± 1.16
11	2494 ± 1
12	377 ± 1
13	1436 ± 1

2.4 Docking Studies

To select among our compounds the best lead candidates and to identify their possible binding modes to human tubulin, we performed different docking simulations using as a target the atomic structures of the polymeric complex formed between Tubulin α , Tubulin β , Stathmin4 and the Tubulin Tyrosine Ligase[28] [PDB code 5J2T]. We compared the binding modes of our moieties to the ones of the known ligands Colchicine and Vinblastine (Figure 10). For all our molecules, we performed a “blind docking”: *i.e.* the docking of small molecules to their targets was done without a priori knowledge of the binding mode of the ligand in the active site of the protein. Our procedure was firstly validated by correctly positioning Vinblastine in its correct binding site, with a RMSD of less than 0.2 Å with respect to the one determined by X-ray crystallography.

The binding site of our moieties is placed on the interface between the alfa and beta subunit of the quaternary assembly of tubulin, in a cleft placed about 7.5Å far from the Vinblastine binding site.

Table 8 reports the residues involved in ligand binding and the binding energies of all the complexes formed by tubulin and our compounds.

Table 8. Binding energies of the complexes formed by tubulin and compounds **5-13** and residues involved in ligand binding.

Compound	Binding Energy (Kcal/mol)	Calculated K_i (μM) *	Tubulin residues involved in ligand binding §	
5	-7.77	2.0	Asp β179, Gln β394	<i>Ala α314, Cys α347, Pro α348, Pro β173, Pro β175, Val β181, Pro β184</i>
6	-8.17	1.02	Asp β179, Gln β394	<i>Ala α314, Cys α347, Pro α348, Pro β173, Pro β175, Val β181, Pro β184</i>
7	-9.48	0.113	Asp β179, Gln β394	<i>Ala α314, Cys α347, Pro α348, Pro β173, Pro β175, Val β181, Pro β184</i>
8	-7.13	5.99	Asp β179	<i>Ala α314, Cys α347, Pro α348, Pro β173, Pro β175, Val β181, Pro β184</i>
9	-8.80	0.357	Asp β179	<i>Ala α314, Cys α347, Pro α348, Pro β173, Pro β175, Val β181, Pro β184</i>
10	-7.25	4.86	Asp β179	<i>Ala α314, Cys α347, Pro α348, Pro β173, Pro β175, Val β181, Pro β184</i>
11	-6.18	29.57	Asp β179, Gln β394	<i>Pro α348, Pro β173, Pro β175, Pro β184</i>
12	-6.33	23.03	Asp β179, Gln β394	<i>Pro α348, Pro β173, Pro β175, Pro β184</i>
13 ⁺	-6.04	37.52	Gln β11, Gln β15	<i>Leu β209, Leu β227</i>

* K_i values as calculated by Autodock algorithm: $K_i = \exp(\Delta G/(R \cdot T))$

§ Residues involved in Hydrogen bond are listed in **bold**. Hydrophobic contacts in *Italic*.

⁺ Binds in a different cleft, on the surface of the beta subunit, out from the dimeric interface

Based on the geometry, the binding energy and the clusterization of the results, we selected as best candidates, molecules **7**, **6** and **9** in ranked order.

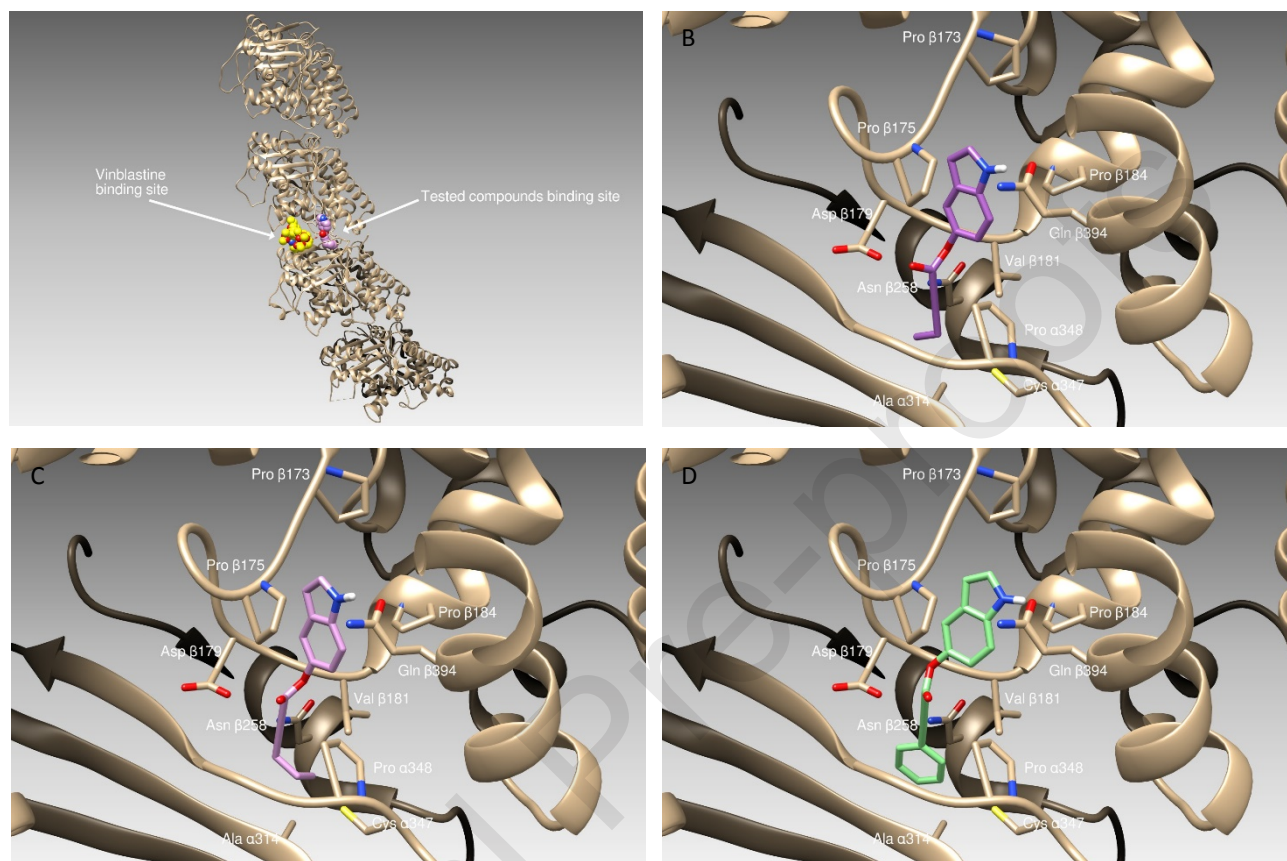


Figure 10. Panel A) A cartoon representation of a Tubulin tetramer (2alpha-2beta subunits). Two different binding sites for the compounds tested are indicated by arrows. Vinblastine and compounds **5-13** binding site are separated by about 11Å. **Panel B)** a more detailed view of compound **5** (violet sticks) binding site. **Panel C)** reports the binding mode of compound **6** (drawn in purple) and **Panel D)** illustrate the pose of compound **7** within the binding site cleft. Residues involved in the binding of the three molecules to tubulin quaternary structure are evidenced and properly labelled.

3. Conclusions

Over the last years, the indole-based compounds have occupied an important position as powerful and versatile pharmacological weapons in the battle against life-threatening diseases as, for instance, cancer. Indeed, several indole derivatives have been employed pre-clinically and clinically and their

multi-target features offered better and more promising therapies, overcoming the drug resistance mechanism and diminishing the undesirable side effects. The assessment of the basic importance of cancer microenvironment have enlarged the number of potential targets hit by indole derivatives and drugs that can control the microtubule assembly by hampering tubulin polymerization or, as well, by obstructing microtubule disassembly, and it could represent pivotal leads to block cancer metastasization. In this paper, we reported the design, the synthesis and the biological evaluation of molecules bearing the indole scaffold. Structure-activity relationships were made, based on the anticancer activities obtained against four cancer cell models (MCF-7, MDA-MB-231, HeLa and Ishikawa). We selected a good lead compound with no effects on the viability of three different normal cells. We proved that compound **7** is able to hamper cancer cells viability, used in these experiments, by blocking the tubulin polymerization reaction, as demonstrated by a direct enzymatic assay and immunostaining studies on the native tubulin. Finally, *in silico* studies corroborated the observed tubulin inhibition. Targeting tubulin, compound **7** lead to cancer cells death by inducing apoptosis. Moreover, we studied the antioxidant properties of this series, finding out that compound **7** can reduce the menadione-induced ROS production in 3T3-L1 cells and that compound **6**, **9** and **10** showed the greatest scavenging activity in DPPH and ABTS assays. We are confident that these outcomes will be exploitable for a better understanding of the great potential of indole derivatives as anticancer drugs.

4. Experimental Protocols

4.1. Chemistry

Chemicals were purchased from Sigma-Aldrich or Lancaster. Yields refer to purified products and were not optimized. Compound structures were confirmed by routine spectrometric and spectroscopic analyses. Melting points were determined on a Gallenkamp melting point apparatus in open glass capillary tubes and are uncorrected. The infrared spectra were recorded on a Perkin-Elmer (Norwalk, CT) Spectrum One FT spectrophotometer and band positions are given in reciprocal centimetres (cm^{-1})

¹H NMR and ¹³C NMR spectra were recorded on a Varian Mercury-VX spectrometer operating at 300 and 75 MHz for ¹H and ¹³C, respectively using CDCl₃ or DMSO-*d*₆ as solvents. Chemical shifts are reported in parts per million (ppm) relative to solvent resonance: δ 7.26 (¹H NMR) and δ 77.3 (¹³C NMR); DMSO-*d*₆, δ 2.48 (¹H NMR) and δ 40.3 (¹³C NMR). *J* values are given in Hz. EI mass spectra were recorded on a Hewlett-Packard 6890-5973 MSD gas chromatograph/mass spectrometer at low resolution. Elemental analyses (C, H, N) were used to confirm the purity of all new compounds and were performed on a Eurovector Euro EA 3000 analyser (results within ± 0.4 of the theoretical values). Chromatographic separations were performed on silica gel columns by flash chromatography (Kieselgel 60, 0.040–0.063 mm, Merck, Darmstadt, Germany). TLC analyses were performed on precoated silica gel on aluminium sheets (Kieselgel 60 F254, Merck).

Synthesis of 5-methoxy-1-methylindole (2). To a stirred cold solution (0 °C) of 5-methoxyindole (**1**) (2.0 g, 13.6 mmol) in dry DMF (60 mL), NaH 60% oil dispersion (0.54 g, 20.4 mmol) was added. After 15 min, iodomethane (2.54 mL, 40.8 mmol) was added and the mixture was further stirred at room temperature for 1 h. Water (200 mL) was then added to the reaction mixture and the solid product obtained was filtered, washed with water and dried to give 2.7 g of pure **2** as a white solid. Yield: 81%; mp: 114–115 °C; GC/MS (70 eV) *m/z* (%): 161 (M⁺, 100). Spectroscopic data were in agreement with the literature[12].

Synthesis of 5-hydroxy-1-methylindole (3). A mixture of 5-methoxy-1-methylindole (**2**, 1.0 g, 6.21 mmol) and anhydrous pyridine hydrochloride (17.9 g, 156 mmol) was heated to melting temperature for 3 h. The reaction mixture was left to cool to room temperature, then ice water was added. The product was extracted with Et₂O. The organic layers were washed with a solution of 2N HCl, dried (Na₂SO₄) and concentrated to give 0.37 g of **3** as a yellow solid. Yield: 46%; mp: 130–132 °C; lit.¹²⁰ 156 °C; GC/MS (70 eV) *m/z* (%): 147 (M⁺, 100). Spectroscopic data were in agreement with the literature [12].

Synthesis of 1H-indol-5-yl pent-2-ynoate (5). To a stirred solution of 5-hydroxyindole (**4**, 0.30 g, 2.3 mmol) in a mixture of CH₂Cl₂ and DMF (10+1 ml), pent-2-ynoic acid (0.24 g, 2.5 mmol),

dicyclohexylcarbodiimide (0.47 g, 2.3 mmol) and dimethyl aminopyridine (0.024 g, 0.2 mmol) were added. The reaction mixture was stirred at room temperature for 4 h, and then concentrated under reduced pressure. The solid residue was suspended in ethyl acetate, filtered and the filtrate was washed with brine. The organic layer was dried over anhydrous Na_2SO_4 and evaporated under reduced pressure. The solid residue was purified by silica gel chromatography (ethyl acetate/hexane 2:8) to give 0.24 g (48%) of a white solid: mp 116–117 °C; IR (KBr): 3386 (NH), 2231 ($\text{C}\equiv\text{C}$), 1706 ($\text{C}=\text{O}$) cm^{-1} ; ^1H NMR (500 MHz, CDCl_3): δ 1.25 (t, $J = 7.3$ Hz, 3H, CH_3), 2.41 (q, $J = 7.3$ Hz, 2H, CH_2), 6.52 (s, 1H, Ar HC), 6.93 (dd, $J = 8.8, 2.4$ Hz, 1H, Ar HC), 7.18 (t, $J = 2.4, 8.8$ Hz, 1H, Ar HC), 7.28 (d, $J = 8.8$ Hz, 1H, Ar HC), 7.37 (d, $J = 1.9$ Hz, 1H, Ar HC), 8.28 (br s, 1H, NH); ^{13}C NMR (125 MHz, CDCl_3): δ 12.5 (1C, CH_2), 12.6 (1C, CH_3), 77.0 (1C, $\text{C}-\text{C}=\text{O}$), 92.9 (1C, $\text{C}-\text{CH}_2$), 102.8 (1C, Ar-C), 111.5 (1C, Ar-C), 112.5 (1C, Ar-C), 115.7 (1C, Ar-C), 125.8 (1C, Ar-C), 128.0 (1C, Ar-C), 133.9 (1C, Ar-C), 143.7 (1C, $\text{C}=\text{O}$), 153.3 (1C, Ar-C); MS (70 eV) m/z (%) 213 (M^+ , 39), 133 (100). Anal. Calcd. for $\text{C}_{13}\text{H}_{11}\text{NO}_2 \cdot 0.25\text{H}_2\text{O}$: C 71.71; H 5.32; N 6.43. Found: C 71.80; H 5.15; N 6.52.

Synthesis of 1H-indol-5-yl hex-2-ynoate (6). Prepared as reported for **5** starting from 5-hydroxyindole (**4**) and *es*-2-ynoic acid. Light brown solid. Yield: 42%; mp 82–83 °C; IR (KBr): 3394 (NH), 2228 ($\text{C}\equiv\text{C}$), 1708 ($\text{C}=\text{O}$) cm^{-1} ; ^1H NMR (500 MHz, CDCl_3): δ 1.04 (t, $J = 7.3$ Hz, 3H, CH_3), 1.61–1.68 (m, 2H, CH_2-CH_3), 2.37 (t, $J = 7.3$ Hz, 2H, CH_2-C), 6.52 (s, 1H, Ar HC-3), 6.93 (dd, $J = 8.8, 2.4$ Hz, 1H, Ar HC), 7.19 (t, $J = 2.9$ Hz, 1H, Ar HC), 7.29 (d, $J = 8.8$ Hz, 1H, Ar HC), 7.37 (d, $J = 1.9$ Hz, 1H, Ar HC), 8.27 (br s, 1H, NH); ^{13}C NMR (125 MHz, CDCl_3): δ 13.5 (1C, CH_3), 20.8 (1C, CH_2-C), 21.0 (1C, CH_2-CH_3), 73.2 (1C, $\text{C}-\text{C}=\text{O}$), 91.8 (1C, $\text{C}-\text{CH}_2$), 102.9 (1C, Ar-C), 111.5 (1C, Ar-C), 112.6 (1C, Ar-C), 115.7 (1C, Ar-C), 125.7 (1C, Ar-C), 128.1 (1C, Ar-C), 133.9 (1C, Ar-C), 143.8 (1C, $\text{C}=\text{O}$), 153.3 (1C, Ar-C); MS (70 eV) m/z (%) 227 (M^+ , 81), 133 (100). Anal. Calcd. for $\text{C}_{14}\text{H}_{13}\text{NO}_2$: C 73.99; H 5.77; N 6.16. Found: C 73.84; H 5.84; N 6.29.

Synthesis of 9-ethylpyrano[3,2-*e*]indol-7(3*H*)-one (11). To a solution of **5** (0.25 g, 1.17 mmol) in a mixture of 1,4-dioxane and 1,2-dichloroethane (6+6 ml), PtCl₄ (0.02 g, 0.06 mmol) was added. The reaction mixture was heated under reflux for 4 h then concentrated under reduced pressure. The residue was dissolved in ethyl acetate and washed with water and brine. The organic layer was then dried (Na₂SO₄) and concentrated under reduced pressure to give a solid residue. The solid product was purified by silica gel chromatography (ethyl acetate/hexane 1:1) to give 40 mg (55%) of a ochre-yellow solid: mp 242–243 °C; IR (KBr): 3253 (NH), 1671 (C=O) cm⁻¹; ¹H NMR (500 MHz, DMSO-*d*₆): δ 1.3 (t, *J* = 7.3 Hz, 3H, CH₃), 3.08 (q, *J* = 7.3 Hz, 2H, CH₂), 6.24 (s, 1H, CH), 6.83 (s, 1H, Ar HC), 7.14 (d, *J* = 8.3 Hz, 1H, Ar HC), 7.59 (t, *J* = 2.9 Hz, 1H, Ar HC), 7.68 (d, *J* = 8.3 Hz, 1H, Ar HC), 11.7 (br s, 1H, NH); ¹³C NMR (125 MHz, DMSO-*d*₆): δ 12.7 (1C, CH₃), 31.1 (1C, CH₂), 103.0 (1C, Ar-C), 111.2 (1C, Ar-C), 111.3 (1C, CH), 116.7 (1C, Ar-C), 122.2 (1C, Ar-C), 128.2 (2C, Ar-C), 133.2 (1C, Ar-C), 150.0 (1C, C-O), 160.3 (1C, C-CH₂), 161.1 (1C, C=O); MS (70 eV) *m/z* (%) 213 (M⁺, 87), 170 (100). Anal. Calcd. for C₁₃H₁₁NO₂·0.34 H₂O: C 71.20; H 5.36; N 6.39. Found: C 71.44; H 5.50; N 6.41.

Synthesis of 9-propylpyrano[3,2-*e*]indol-7(3*H*)-one (12). Prepared as reported for **11** starting from **6**. Ochre-yellow solid. Yield: 16%; mp 234–235 °C; IR (KBr): 3188 (NH), 1667 (C=O) cm⁻¹; ¹H NMR (500 MHz, DMSO-*d*₆): δ 1.03 (t, *J* = 7.3 Hz, 3H, CH₃), 1.66–1.74 (m, 2H, CH₂), 2.98 (t, *J* = 7.3 Hz, 2H, CH₂C), 6.23 (s, 1H, CH), 6.75 (s, 1H, Ar HC), 7.13 (d, *J* = 8.8 Hz, 1H, Ar HC), 7.59 (t, *J* = 2.9 Hz, 1H, Ar HC), 7.68 (d, *J* = 8.8 Hz, 1H, Ar HC), 11.7 (br s, 1H, NH); ¹³C NMR (125 MHz, DMSO-*d*₆): δ 14.1 (1C, CH₃), 21.4 (1C, CH₂-CH₃), 36.6 (1C, CH₂-C), 102.7 (1C, Ar-C), 111.2 (1C, Ar-C), 111.3 (1C, Ar-C), 112.4 (1C, CH), 116.8 (1C, Ar-C), 122.2 (1C, Ar-C), 128.2 (1C, Ar-C), 133.3 (1C, Ar-C), 150.2 (1C, C-O), 158.6 (1C, C-CH₂), 161.0 (1C, C=O); MS (70 eV) *m/z* (%) 227 (M⁺, 100). Anal. Calcd. for C₁₄H₁₃NO₂·0.34 H₂O: C 72.09; H 5.91; N 6.00; N 6.39. Found: C 71.83; H 5.87; N 5.86.

Synthesis of 1H-indol-5-yl 3-phenylprop-2-ynoate (7). Prepared as reported for **5** starting from 5-hydroxyindole (**4**) and phenylpropionic acid. Light beige solid. Yield: 40%; mp 142–143 °C; IR (KBr): 3409 (NH), 2221 (C≡C), 1705 (C=O) cm⁻¹; ¹H NMR (500 MHz, CDCl₃): δ 6.56 (s, 1H, Ar HC), 7.0 (dd, *J* = 8.8, 1.9 Hz, 1H, Ar HC), 7.22–7.28 (m, 1H, Ar HC), 7.36–7.50 (m, 6H, Ar HC), 7.62 (d, *J* = 7.8 Hz, 1H, Ar HC), 8.26 (br s, 1H, NH); ¹³C NMR (125 MHz, CDCl₃): δ 80.6 (1C, C=C=O), 88.4 (1C, C-CH₂), 103.1 (1C, Ar-C), 111.5 (1C, Ar-C), 112.7 (1C, Ar-C), 115.8 (1C, Ar-C), 119.5 (1C, Ar-C), 125.7 (C, Ar-C), 128.2 (1C, Ar-C), 128.6 (2C, Ar-C), 130.9 (1C, Ar-C), 133.2 (2C, Ar-C), 133.9 (1C, Ar-C), 143.9 (1C, C=O), 153.5 (1C, Ar-C); MS (70 eV) *m/z* (%) 261 (M⁺, 23), 129 (100). Anal. Calcd. for C₁₇H₁₁NO₂·0.17 H₂O: C 77.41; H 4.50; N 5.21; N 6.39. Found: C 77.70; H 4.37; N 5.47.

Synthesis of 1-methyl-1H-indol-5-yl pent-2-ynoate (8). Prepared as reported for **5** starting from 5-methoxyindole (**3**) and pent-2-ynoic acid. Tan solid. Yield: 40%; mp 47–48 °C; IR (KBr): 2221 (C≡C), 1723 (C=O) cm⁻¹; ¹H NMR (300 MHz, CDCl₃): δ 1.25 (t, *J* = 1.1 Hz, 3H, CH₂CH₃), 2.40 (q, *J* = 6.4 Hz, 2H, CH₂), 3.80 (s, *J* = 1.1 Hz, 3H, NCH₃), 6.46 (d, *J* = 2.9 Hz, 1H, Ar HC), 6.97 (dd, *J* = 8.7, 2.3 Hz, 1H, Ar HC), 7.08 (d, *J* = 2.9 Hz, 1H, Ar HC), 7.25–7.35 (m, 2H, Ar HC); ¹³C NMR (75 MHz, CDCl₃): δ 12.5 (1C, CH₂-C), 12.6 (1C, CH₃-CH₂), 33.0 (1C, CH₃-N), 72.5 (1C, C=CO), 92.6 (1C, C-CH₂), 101.3 (1C, Ar-C), 109.6 (1C, Ar-C), 112.8 (1C, Ar-C), 115.3 (1C, Ar-C), 128.6 (2C, Ar-C), 130.2 (1C, Ar-C), 134.8 (1C, C=O), 143.6 (1C, C-O); MS (70 eV) *m/z* (%) 227 (M⁺, 41); 147 (100). Anal. Calcd. for C₁₄H₁₃NO₂·0.20 H₂O: C 72.84; H 5.85; N 6.07. Found: C 72.87; H 5.77; N 6.22.

Synthesis of 9-ethyl-3-methylpyrano[3,2-*e*]indol-7(3H)-one (13). Prepared as reported for **11** starting from **8**. Tan solid. Yield: 62%; mp 174–175 °C; IR (KBr): 1630 (C=O) cm⁻¹; ¹H NMR (300 MHz, CDCl₃): δ 1.41 (t, *J* = 7.0 Hz, 3H, CH₂CH₃), 3.13 (q, *J* = 5.8 Hz, 2H, CH₂), 3.87 (s, 3H, NCH₃), 6.32 (s, 1H, CH), 6.82 (d, *J* = 4.1 Hz, 1H, Ar HC), 7.23–7.28 (m, 2H, Ar HC), 7.5 (d, *J* = 8.7 Hz, 1H,

Ar HC); ^{13}C NMR (75 MHz, CDCl_3): δ 12.1 (1C, $\text{CH}_3\text{-CH}_2$), 28.0 (1C, $\text{CH}_3\text{-N}$), 30.8 (1C, CH_2), 100.4 (1C), 102.2 (1C, Ar-C), 111.8 (1C, Ar-C), 111.9 (1C, Ar-C), 113.4 (1C, Ar-C), 119.3 (2C, Ar-C), 130.4 (2C, C-O + CH), 159.5 (1C, C- CH_2), 163.4 (1C, C=O); MS (70 eV) m/z (%) 227 (M^+ , 100). Anal. Calcd. for $\text{C}_{14}\text{H}_{13}\text{NO}_2$: C 73.99; H 5.77; N 6.16. Found: C 73.79; H 5.85; N 6.13.

Synthesis of 1-methyl-1H-indol-5-yl hex-2-ynoate (9). Prepared as reported for **5** starting from 5-methoxyindole (**3**) and es-2-ynoic acid. Slightly yellowish oil. Yield: 11%; ^1H NMR (300 MHz, CDCl_3): δ 1.04 (t, $J = 7.0$ Hz, 3H, CH_2CH_3), 1.65 (q, $J = 7.0$ Hz, 2H, CH_2CH_3), 2.37 (t, $J = 7.0$ Hz, 2H, C CH_2), 3.77 (s, 3H, NCH_3), 6.46 (d, $J = 2.9$ Hz, 1H, Ar HC), 6.97 (dd, $J = 8.8, 2.3$ Hz, 1H, Ar HC), 7.08 (d, $J = 3.5$ Hz, 1H, Ar HC), 7.29 (d, $J = 8.8$ Hz, 1H, Ar HC), 7.35 (d, $J = 2.3$ Hz, 1H, Ar HC); ^{13}C NMR (75 MHz, CDCl_3): δ 13.4 (1C, $\text{CH}_3\text{-CH}_2$), 20.7 (1C, $\text{CH}_2\text{-C}$), 21.0 (1C, $\text{CH}_2\text{-CH}_3$), 33.0 (1C, $\text{CH}_3\text{-N}$), 73.1 (1C, C=CO), 91.5 (1C, C- CH_2), 101.3 (1C, Ar-C), 109.6 (1C, Ar-C), 112.8 (1C, Ar-C), 115.3 (1C, Ar-C), 128.6 (1C, Ar-C), 130.1 (1C, Ar-C), 134.8 (1C, Ar-C), 143.7 (1C, C=O), 153.1 (1C, C-O); MS (70 eV) m/z (%) 241 (M^+ , 33), 147 (100).

Synthesis of 1-methyl-1H-indol-5-yl 3-phenylprop-2-ynoate (10). Prepared as reported for **5** starting from 5-methoxyindole (**3**) and phenylpropionic acid. Brown oil. Yield: 34%; IR (NaCl): 2222 ($\text{C}\equiv\text{C}$), 1723 ($\text{C}=\text{O}$) cm^{-1} ; ^1H NMR (500 MHz, CDCl_3): δ 3.79 (s, 3H, CH_3), 6.50 (s, 1H, HC), 7.06 (d, $J = 8.8$ Hz, 1H, Ar HC), 7.10 (s, 1H, Ar HC), 7.32 (d, $J = 8.8$ Hz, 1H, Ar HC), 7.38–7.52 (m, 5H, Ar HC), 7.64 (d, $J = 7.3$ Hz, 2H, Ar HC); ^{13}C NMR (125 MHz, CDCl_3): δ 33.1 (1C, CH_3), 80.7 (1C, C=CO), 88.2 (1C, C- CH_2), 101.3 (1C, Ar-C), 109.7 (1C, Ar-C), 112.8 (1C, Ar-C), 115.3 (1C, Ar-C), 119.5 (1C, Ar-C), 128.6 (1C, Ar-C), 128.7 (2C, Ar-C), 130.3 (1C, Ar-C), 130.9 (1C, Ar-C), 133.2 (2C, Ar-C), 134.9 (1C, Ar-C), 143.7 (1C, C=O), 153.5 (1C, C-O); MS (70 eV) m/z (%) 275 (M^+ , 38), 129 (100).

4.1.2 Thermal stability test

20 mg of **7** were heated in a reaction flask in oil bath for 6 hours at 60 °C.

4.2 Biology

4.2.1 Cell culture

The six cell lines used in this work (MCF-7, MDA-MB-231, HeLa, ISHIKAWA, MCF-10A and HEK-293) were purchased from American Type Culture Collection (ATCC, Manassas, VA, USA). All cell lines were maintained at 37 °C in a humidified atmosphere of 95% air and 5% CO₂ and periodically screened for contamination. MCF-7, human breast cancer cells estrogen receptor (ER)-positive, and human breast cancer triple negative MDA-MB231 were grown in DMEM-F12 medium containing 2 mmol/L L-glutamine, 1 mg/mL penicillin-streptomycin and 5% Newborn Calf Serum (NCS) or 5% Fetal Bovine Serum (FBS), respectively. HeLa (human epithelial cervix carcinoma cells), estrogen receptor (ER)-negative, and Ishikawa (human endometrial adenocarcinoma cells), estrogen receptor (ER)-positive, were cultured in MEM (minimum essential Eagle's Medium) supplemented with 10% FBS, 1% L-glutamine, 100 U/mL penicillin/streptomycin and 1% Non-Essential Amino Acids (NEAA). MCF-10A human mammary epithelial cells were cultured in DMEM/F12 medium, supplemented with 5% horse serum (HS) (Eurobio, Les Ullis, Cedex, France), 100 U/mL penicillin/streptomycin, 0.5 mg/mL hydrocortisone, 20 ng/mL hEGF (human epidermal growth factor), 10 mg/mL insulin and 0.1 mg/mL cholera enterotoxin (Sigma-Aldrich, Milano, Italy). HEK-293, human embryonic kidney cells, were cultured in DMEM high glucose supplemented with 10% FBS, 1% L-glutamine and 100 U/mL penicillin/streptomycin.

4.2.2 MTT assay

The *in vitro* antiproliferative activities of all the target compounds were determined by a MTT (Sigma) assay [29, 30]. Briefly, approximately cells were seeded in a 48-well plate and were grown in full medium. Before being treated, cells have been starved in serum free medium for 24 h for allowing cell cycle synchronization. After cells were exposed to compounds of differing concentrations (0,1-1-10-20-40 μM) for 24 h. Then to the treatment cells, MTT (3-(4,5-dimethylthiazol-2-yl)-2,5-diphenyl tetrazolium bromide) was added to each well (final concentration

(0.5 mg/mL), followed by incubation for 2 h at 37 °C. After incubation, the supernatant from each well was carefully removed and the formazan crystals were dissolved in 200 µL of DMSO and then optical density was measured at 570 nm using a microplate reader. Results are represented as percent (%) of basal and the IC₅₀ values were calculated using GraphPad Prism 6 (GraphPad Software, La Jolla, CA, USA).

4.2.3 Cytoskeleton and mitochondrial staining and immunofluorescence

Cells were added in 48-well culture plates containing glass slides and allowed to attach overnight at 37 °C in 5% CO₂, then serum-deprived for 24h and exposed to compounds for 24h (concentration equal to its IC₅₀ value). Then, the cells after PBS-washed, were fixed with cold methanol, for 15 min at -20°C, and incubated with primary antibody, diluted in blocking solution overnight at 4°C, as previously described [20]. The rabbit anti-β-Tubulin (9104) were purchased from Santa Cruz Biotechnology and used at 1:100 dilution. Coverslips were then washed 3 times with PBS, then the secondary antibody Alexa Fluor® 488 conjugate goat-anti-rabbit (1:500, Thermo Fisher Scientific, MA, USA) was added and incubated for 2h at 37 °C. Nuclei were stained using DAPI (Sigma Aldrich, Mila, Italy) for 10 min at a concentration of 0.2 µg/mL then washed 3 times with PBS. Fluorescence was detected using a fluorescence microscope (Leica DM 6000). LAS-X software was used to acquire and process all images.

4.2.4 Tubulin polymerization assay

Tubulin polymerization inhibition was measured using *in vitro* Tubulin Polymerization Assay Kit purchased from EMD Millipore Corporation[22]. Polymerization reactions occur in 70 µL final volumes, of which 60 µL is the 60 µM tubulin in 1xPB-GTP and 10 µL is the test substance dissolved in 1 x PB-GTP. Paclitaxel, Vinblastine (used as control) and compound **7**, were dissolved in DMSO and used at final concentration of 10 µM. These reactive were combined in 96-well plate on ice. After the plate was transferred into the spectrophotometer pre-warmed at 37 °C and the turbidity variation

was measured every 30 seconds at 350 nm for 90 minutes. The plate was shaken for 10 seconds before each measurement. Turbidity (absorbance) readings were used to calculate the extent of polymerization [% inhibition = $(1 - A_{350 \text{ sample}}/A_{350 \text{ control}}) \times 100$].

4.2.4 TUNEL assay

Apoptosis was detected by the TUNEL assay, according to the guidelines of the manufacturer (CFTM488A TUNEL Assay Apoptosis Detection Kit, Biotium, Hayward, CA). The cells were grown on glass coverslips and, after treatment, they were washed three times with PBS, then methanol-fixed at -20 °C for 15 min. After three washes with 0.01% (v/v) Triton X-100 in PBS, they were incubated with 100 mL of TUNEL equilibration buffer for 5 min. After its removal, 50 mL of TUNEL reaction mixture containing 1 mL of terminal deoxynucleotidyl transferase (TdT) were added to each sample and incubated in a dark and humidified chamber for 2 h at 37 °C. Samples were washed three-times with ice-cold PBS containing 0.1% Triton X-100 and 5 mg/mL bovine serum albumin. DAPI (Sigma, 0.2 mg/mL) counterstain was performed for 10 min at 37 °C under dark and humidified conditions. Fixed cells were then washed three times with cold PBS (0.5 mL), adding one drop of mounting solution, and were observed and imaged under a fluorescence microscope (Leica DM6000; 20x magnification) with excitation/emission wavelength maxima of 490/515 nm (CF 488A) or 350/460 nm (DAPI). Images are representative of three independent experiments.

4.2.5 Detection of intracellular H₂O₂

Cells were grown in 48-well plates and then co-treated with the tested compounds and with menadione (Sigma-Aldrich), used to induce ROS production [31]. After treatment, cells were washed with PBS and 10 μM 2',7'-dichlorofluorescein diacetate (Sigma-Aldrich) was added for 40 min, and then incubated at 37 °C, 5% CO₂. In presence of intracellular H₂O₂, non-fluorescent 2',7'-dichlorofluorescein diacetate (DCF-DA) is oxidized and converted to green fluorescent 2',7'-dichlorofluorescein (DCF). Then, cells were fixed and processed, as already described [2]. At the end

cells were observed and imaged under a fluorescence microscope (Leica DM6000; 20 × magnification) with excitation/emission wavelength of 490 nm/515 nm (DCF) or 350 nm/460 nm (DAPI). Images are representative of three independent experiments. The increase or the decrease of ROS generation in the treated cells, shown as green fluorescence, was quantified using ImageJ.

4.3 Antioxidant activity

4.3.1 DPPH Assay

The free radical scavenging capacity of all compounds (**5–13**) was determined by DPPH assay according to a known protocol [32] at four different concentrations (2.5, 1.0, 0.5 and 0.1 mg mL⁻¹ in DMSO)

More specifically, standard DMSO solutions (2.5, 1.0, 0.5 and 0.1 mg mL⁻¹ DMSO) of all compounds were prepared. 0.1 mL of each solution was mixed with 0.1 mL of DPPH solution (1 mM in MeOH) and 2.8 mL of MeOH to give the final volume of 3 mL, so as to obtain four different solutions with concentrations of 8.33, 3.33, 1.67, 0.33 µg mL⁻¹ for each compound. The mixtures were shaken vigorously and incubated for 30 min at room temperature in the dark. The colorimetric decrease in absorbance of each sample was quantified spectrophotometrically at 517 nm against a blank (3 mL of MeOH) using a UV–vis spectrophotometer (model V-550, Jasco Europe). The control was a DPPH solution (2.8 mL of MeOH, 0.1 mL of DPPH 1 mM, 0.1 mL DMSO). Experiments were carried out in triplicate, and the results were expressed as a percentage of free radical inhibition (%I_{DPPH}), according to the formula:

$$\%I_{\text{DPPH}} = \frac{\text{Absorbance}_{517\text{nm of control}} - \text{Absorbance}_{517\text{nm of sample}}}{\text{Absorbance}_{517\text{nm of control}}} \times 100$$

The inhibition percentage values (%I_{DPPH}) were used to calculate EC₅₀ values by GraphPad Prism 8 software (GraphPad Inc., San Diego, CA). Trolox was used as the reference compound to build a

calibration curve ($33-0.003 \mu\text{g mL}^{-1}$). and the results were also expressed as μg of Trolox Equivalent per gram of dry sample weight ($\mu\text{g TE/g DW}$) (TEAC).

4.3.2. ABTS Assay

The radical scavenging effects of all compounds on a 2,2'-azino-bis(3-ethylbenzothiazoline-6-sulfonate) radical cation ($\text{ABTS}^{\bullet+}$) were evaluated according to a known protocol[33].

Briefly, $\text{ABTS}^{\bullet+}$ radical stock solution was prepared by mixing 50 mL of 2 mM ABTS and 0.5 mL of 70 mM $\text{K}_2\text{S}_2\text{O}_8$ and allowing the solution to stand in the dark at room temperature for 16 h before use. The $\text{ABTS}^{\bullet+}$ solution was diluted with absolute ethanol to yield the absorbance of 0.70 ± 0.02 at 734 nm. Compounds solutions (2.5, 1.0, 0.5 and 0.1 mg mL^{-1} DMSO) were prepared and then 0.03 mL of each one was mixed with 3 mL of the $\text{ABTS}^{\bullet+}$ solution obtaining the final concentrations of 25, 10, 5, 1 $\mu\text{g mL}^{-1}$. Then the mixtures were kept in the dark and under stirring for 5 min before absorbance at 734 nm was measured. Experiments were carried out in triplicate. The control was an ABTS solution (0.03 mL of DMSO, 3 mL of ABTS).

The ABTS radical scavenging was expressed as ($\%I_{\text{ABTS}}$) compared to the control according to the formula:

$$\% I_{\text{ABTS}} = \frac{\text{Absorbance } 734\text{nm of control} - \text{Absorbance } 734\text{nm of sample}}{\text{Absorbance } 734\text{nm of control}} \times 100$$

E_{C50} values were calculated using GraphPad Prism 8 software (GraphPad Inc., San Diego, CA). Trolox was used as the reference compound to build a calibration curve and the results were expressed also as per gram of dry sample weight ($\mu\text{g TE/g DW}$) (TEAC).

4.3.4 ROS protection assay

For the evaluation of the protective role of the molecules against oxidative stress, 3T3-L1 mouse fibroblasts cells were grown in 48-well plates and then treated with the compounds to test, menadione (Sigma-Aldrich), which causes ROS production[31]. After treatment, cells were washed with PBS

and 10 μM of 2',7'-dichlorofluorescein diacetate (Sigma-Aldrich) was added for 40 min, and then incubated at 37 ° C, 5% CO_2 . In presence of intracellular H_2O_2 , nonfluorescent 2',7'-dichlorofluorescein diacetate (DCF-DA) is oxidized and converted to green fluorescent 2',7'-dichlorofluorescein (DCF)[2]. Then, cells were washed with PBS and methanol-fixed at -20 °C for 15 min. After three washes with ice-cold PBS, 2-(4-amidinophenyl)-6- indole carbamidine dihydrochloride (DAPI; 0.2 mg mL^{-1}) counterstain was performed for 10 min at 37 °C under dark conditions. Cells were then washed three-times with cold PBS, one drop of mounting solution was added, and then they were observed and imaged under a fluorescence microscope (Leica DM6000; 20 \times magnification) with excitation/emission wavelength maxima of 490 nm/515 nm (DCF) or 350 nm/460 nm (DAPI). Images are representative of three independent experiments. The increase or the decrease of ROS generation in treated cells, shown as green fluorescence, was quantified using ImageJ.

4.4 Docking

Docking simulations were performed using the program Autodock v.4.2.2.[34]. All the simulations were performed using the program defaults and a searching grid encompassing the whole protein volume. Each docking experiment consisted of 100 Lamarckian Genetic Algorithm runs. The generated docking poses were ranked in order of increasing docking energy values and clustered based on a RMSD cut-off value of 1.0 Å. From the structural analysis of the lowest energy solutions of each cluster, we could highlight the protein binding site. As targets for all the simulations we used: the molecular structure of the assembly formed by Tubulin α , Tubulin β , Stathmin4 and the Tubulin Tyrosine Ligase[28] [PDB code 5J2T]. Figure 10 was drawn with the program Chimera [35].

References

- [1] A. Fazio, D. Iacopetta, C. La Torre, J. Ceramella, N. Muia, A. Catalano, A. Carocci, M.S. Sinicropi, Finding solutions for agricultural wastes: antioxidant and antitumor properties of pomegranate Akko peel extracts and beta-glucan recovery, *Food Funct* 9(12) (2018) 6618-6631.
- [2] D. Iacopetta, F. Grande, A. Caruso, R.A. Mordocco, M.R. Plutino, L. Scrivano, J. Ceramella, N. Muia, C. Saturnino, F. Puoci, C. Rosano, M.S. Sinicropi, New insights for the use of quercetin analogs in cancer treatment, *Future Med Chem* 9(17) (2017) 2011-2028.
- [3] S. Dadashpour, S. Emami, Indole in the target-based design of anticancer agents: A versatile scaffold with diverse mechanisms, *Eur J Med Chem* 150 (2018) 9-29.
- [4] W.A. Creasey, Vinca Alkaloids and Colchicine, in: S. A.C., J. D.G. (Eds.), *Antineoplastic and Immunosuppressive Agents II*, Springer, Berlin, Heidelberg, 1975, pp. 686-694.
- [5] F. Roussi, F. Guéritte, J. Fahy, The Vinca Alkaloids, in: G.M. Cragg, D.G. Kingston, D.J. Newman (Eds.), *Anticancer Agents from Natural Products*, CRC/Taylor & Francis, Boca Raton, Florida, 2012, pp. 177-198.
- [6] B.P. Bandgar, L.K. Adsul, S.V. Lonikar, H.V. Chavan, S.N. Shringare, S.A. Patil, S.S. Jalde, B.A. Koti, N.A. Dhole, R.N. Gacche, A. Shirfule, Synthesis of novel carbazole chalcones as radical scavenger, antimicrobial and cancer chemopreventive agents, *J Enzyme Inhib Med Chem* 28(3) (2013) 593-600.
- [7] A. Brancale, R. Silvestri, Indole, a core nucleus for potent inhibitors of tubulin polymerization, *Med Res Rev* 27(2) (2007) 209-38.
- [8] H.J. Park, H.J. Lee, E.J. Lee, H.J. Hwang, S.H. Shin, M.E. Suh, C. Kim, H.J. Kim, E.K. Seo, S.K. Lee, Cytotoxicity and DNA topoisomerase inhibitory activity of benz[f]indole-4,9-dione analogs, *Biosci Biotechnol Biochem* 67(9) (2003) 1944-9.
- [9] S. Adler, G. Rashid, A. Klein, Indole-3-carbinol inhibits telomerase activity and gene expression in prostate cancer cell lines, *Anticancer Res* 31(11) (2011) 3733-7.
- [10] D. Fanale, G. Bronte, F. Passiglia, V. Calo, M. Castiglia, F. Di Piazza, N. Barraco, A. Cangemi, M.T. Catarella, L. Insalaco, A. Listi, R. Maragliano, D. Massihnia, A. Perez, F. Toia, G. Cicero, V. Bazan, Stabilizing versus destabilizing the microtubules: a double-edge sword for an effective cancer treatment option?, *Anal Cell Pathol (Amst)* 2015 (2015) 690916.

- [11] K. Sakchaisri, S.O. Kim, J. Hwang, N.K. Soung, K.H. Lee, T.W. Choi, Y. Lee, C.M. Park, N.R. Thimmegowda, P.Y. Lee, B. Shwetha, G. Srinivasrao, T.T. Pham, J.H. Jang, H.W. Yum, Y.J. Surh, K.S. Lee, H. Park, S.J. Kim, Y.T. Kwon, J.S. Ahn, B.Y. Kim, Anticancer activity of a novel small molecule tubulin inhibitor STK899704, *PLoS One* 12(3) (2017) e0173311.
- [12] M.S. Sinicropi, A. Caruso, F. Conforti, M. Marrelli, H. El Kashef, J.C. Lancelot, S. Rault, G.A. Statti, F. Menichini, Synthesis, inhibition of NO production and antiproliferative activities of some indole derivatives, *J Enzyme Inhib Med Chem* 24(5) (2009) 1148-53.
- [13] L. Jin, M. Qi, D.Z. Chen, A. Anderson, G.Y. Yang, J.M. Arbeit, K.J. Auburn, Indole-3-carbinol prevents cervical cancer in human papilloma virus type 16 (HPV16) transgenic mice, *Cancer Res* 59(16) (1999) 3991-7.
- [14] H. Leong, G.L. Firestone, L.F. Bjeldanes, Cytostatic effects of 3,3'-diindolylmethane in human endometrial cancer cells result from an estrogen receptor-mediated increase in transforming growth factor-alpha expression, *Carcinogenesis* 22(11) (2001) 1809-17.
- [15] L.M. Howells, B. Gallacher-Horley, C.E. Houghton, M.M. Manson, E.A. Hudson, Indole-3-carbinol inhibits protein kinase B/Akt and induces apoptosis in the human breast tumor cell line MDA MB468 but not in the nontumorigenic HBL100 line, *Mol Cancer Ther* 1(13) (2002) 1161-72.
- [16] C. Hong, G.L. Firestone, L.F. Bjeldanes, Bcl-2 family-mediated apoptotic effects of 3,3'-diindolylmethane (DIM) in human breast cancer cells, *Biochem Pharmacol* 63(6) (2002) 1085-97.
- [17] K.S. Prasad, R.R. Pillai, M.P. Ghimire, R. Ray, M. Richter, C. Shivamallu, A.S. Jain, S.K. Prasad, P. Sushma, S. Armakovic, S.J. Armakovic, R.G. Amachawadi, Indole moiety induced biological potency in pseudo -peptides derived from 2-amino-2-(1H-indole-2-yl) based acetamides: Chemical synthesis, in vitro anticancer activity and theoretical studies, *Journal of Molecular Structure* 1217 (2020).
- [18] R.L. Siegel, K.D. Miller, A. Jemal, Cancer statistics, 2016, *CA Cancer J Clin* 66(1) (2016) 7-30.
- [19] I.B. Johns, E.A. McElhill, J.O. Smith, Thermal Stability of Some Organic Compounds., *J. Chem. Eng. Data* 7(2) (1962) 277-281.
- [20] J. Ceramella, M.R. Loizzo, D. Iacopetta, M. Bonesi, V. Sicari, T.M. Pellicano, C. Saturnino, A. Malzert-Freon, R. Tundis, M.S. Sinicropi, *Anchusa azurea* Mill. (Boraginaceae) aerial parts methanol extract

interfering with cytoskeleton organization induces programmed cancer cells death, *Food Funct* 10(7) (2019) 4280-4290.

[21] R. Kaur, G. Kaur, R.K. Gill, R. Soni, J. Bariwal, Recent developments in tubulin polymerization inhibitors: An overview, *Eur J Med Chem* 87 (2014) 89-124.

[22] D. Iacopetta, C. Rosano, M. Sirignano, A. Mariconda, J. Ceramella, M. Ponassi, C. Saturnino, M.S. Sinicropi, P. Longo, Is the Way to Fight Cancer Paved with Gold? Metal-Based Carbene Complexes with Multiple and Fascinating Biological Features, *Pharmaceuticals (Basel)* 13(5) (2020).

[23] H. Aryapour, G.H. Riazi, S. Ahmadian, A. Foroumadi, M. Mahdavi, S. Emami, Induction of apoptosis through tubulin inhibition in human cancer cells by new chromene-based chalcones, *Pharm Biol* 50(12) (2012) 1551-60.

[24] J.H. Hwang, M. Takagi, H. Murakami, Y. Sekido, K. Shin-ya, Induction of tubulin polymerization and apoptosis in malignant mesothelioma cells by a new compound JBIR-23, *Cancer Lett* 300(2) (2011) 189-96.

[25] F.L. Kiechle, X. Zhang, Apoptosis: biochemical aspects and clinical implications, *Clin Chim Acta* 326(1-2) (2002) 27-45.

[26] M. Redza-Dutordoir, D.A. Averill-Bates, Activation of apoptosis signalling pathways by reactive oxygen species, *Biochim Biophys Acta* 1863(12) (2016) 2977-2992.

[27] A. Floegel, D.-O. Kim, S.-J. Chung, S.I. Koo, O.K. Chun, Comparison of ABTS/DPPH assays to measure antioxidant capacity in popular antioxidant-rich US foods, *J Food Compos Anal* 24 (2011) 1043-1048.

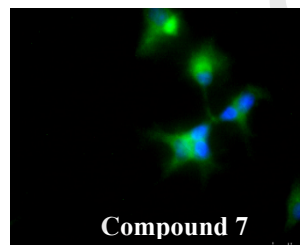
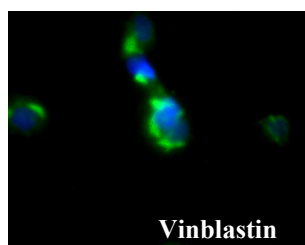
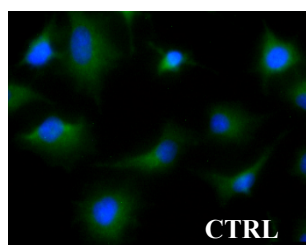
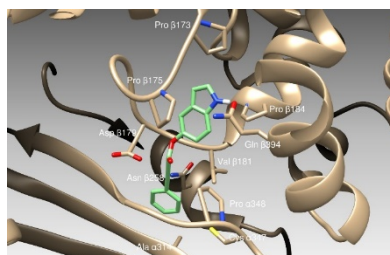
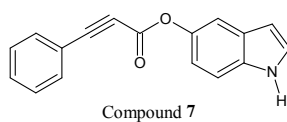
[28] A.B. Waight, K. Bargsten, S. Doronina, M.O. Steinmetz, D. Sussman, A.E. Protta, Structural Basis of Microtubule Destabilization by Potent Auristatin Anti-Mitotics, *PLoS One* 11(8) (2016) e0160890.

[29] D. Iacopetta, C. Rosano, F. Puoci, O.I. Parisi, C. Saturnino, A. Caruso, P. Longo, J. Ceramella, A. Malzert-Freon, P. Dallemagne, S. Rault, M.S. Sinicropi, Multifaceted properties of 1,4-dimethylcarbazoles: Focus on trimethoxybenzamide and trimethoxyphenylurea derivatives as novel human topoisomerase II inhibitors, *Eur J Pharm Sci* 96 (2017) 263-272.

[30] A. Fazio, C. La Torre, M.C. Caroleo, P. Caputo, P. Plastina, E. Cione, Isolation and Purification of Glucans from an Italian Cultivar of *Ziziphus jujuba* Mill. and In Vitro Effect on Skin Repair, *Molecules* 25(4) (2020).

- [31] D.N. Criddle, S. Gillies, H.K. Baumgartner-Wilson, M. Jaffar, E.C. Chinje, S. Passmore, M. Chvanov, S. Barrow, O.V. Gerasimenko, A.V. Tepikin, R. Sutton, O.H. Petersen, Menadione-induced reactive oxygen species generation via redox cycling promotes apoptosis of murine pancreatic acinar cells, *J Biol Chem* 281(52) (2006) 40485-92.
- [32] P. Plastina, A. Fazio, B. Gabriele, Comparison of fatty acid profile and antioxidant potential of extracts of seven Citrus rootstock seeds, *Nat Prod Res* 26(23) (2012) 2182-7.
- [33] M. Leporini, M.R. Loizzo, R. Tundis, C. La Torre, A. Fazio, P. Plastina, Non-Pungent n-3 Polyunsaturated Fatty Acid (PUFA)-Derived Capsaicin Analogues as Potential Functional Ingredients with Antioxidant and Carbohydrate-Hydrolysing Enzyme Inhibitory Activities, *Antioxidants (Basel)* 8(6) (2019).
- [34] G.M. Morris, R. Huey, W. Lindstrom, M.F. Sanner, R.K. Belew, D.S. Goodsell, A.J. Olson, AutoDock4 and AutoDockTools4: Automated docking with selective receptor flexibility, *J Comput Chem* 30(16) (2009) 2785-91.
- [35] E.F. Pettersen, T.D. Goddard, C.C. Huang, G.S. Couch, D.M. Greenblatt, E.C. Meng, T.E. Ferrin, UCSF Chimera--a visualization system for exploratory research and analysis, *J Comput Chem* 25(13) (2004) 1605-12.

Graphical abstract



Highlights

- Synthesis of new indole and pyranoindole derivatives with anticancer activity
- 1*H*-indol-5-yl 3-phenylprop-2-ynoate (**7**) exhibited good antitumor activity against HeLa cancer cell line.
- Compound **7** can kill selectively the cancer cells by blocking the tubulin polymerization reaction
- *In silico* studies corroborated the observed tubulin inhibition
- Compound **7** can reduce the menadione-induced ROS production in 3T3-L1 cells

Declaration of interests

The authors declare that they have no known competing financial interests or personal relationships that could have appeared to influence the work reported in this paper.

The authors declare the following financial interests/personal relationships which may be considered as potential competing interests: